Thermally activated crack fronts propagating in pinning disorder: simultaneous brittle/creep behavior depending on scale

Alain Cochard, Olivier Lengliné, Knut Jørgen Måløy, Renaud Toussaint

PHILOSOPHICAL TRANSACTIONS A

rsta.royalsocietypublishing.org

Research

Article submitted to journal

Subject Areas:
fracture, activation, brittle/creep

Keywords:
pinning, thermal, scaling

Author for correspondence:
Insert corresponding author name
e-mail: renaud.toussaint@unistra.fr

THE ROYAL SOCIETY PUBLISHING

Thermally activated crack fronts propagating in pinning disorder: simultaneous brittle/creep behavior depending on scale

A. Cochard[1], O. Lengliné[1], K.J. Måløy[2] and R. Toussaint[1,2]

[1]Institut de Physique du Globe de Strasbourg, UMR7516 CNRS, Université de Strasbourg/EOST, Strasbourg, France

[2]PoreLab, The Njord Center, Department of Physics, University of Oslo, Blindern, Oslo, Norway

We study theoretically the propagation of a crack front in mode I along an interface in a disordered elastic medium, with a numerical model considering a thermally activated rheology, toughness disorder, and long range elastic interactions. This model reproduces the large scale dynamics of the crack front position in fast or creep loading regimes, but also the small scale self-affine behavior of the front. Two different scaling laws are predicted for the front morphology, with a Hurst exponent of 0.5 at small scales, and a logarithmic scaling law at large scales, consistently with experiments. The prefactor of these scaling laws is expressed as function of the temperature, and of the quenched disorder characteristics. The cross-over between these regimes is expressed as function of the quenched disorder amplitude, is proportional to the average energy release rate, and to the inverse of temperature. This model captures as well the experimentally observed local velocity fluctuations probability distribution, with a high velocity tail $P(v) \sim v^{-2.6}$. This feature is shown to arise when the quenched disorder is sufficiently large, whereas smaller toughness fluctuations lead to a lognormal-like velocity distribution. Overall, the system is shown to obey a scaling determined by two distinct mechanisms as function of scale: namely, the large scales display fluctuations similar to an elastic line in an annealed noise excited as the average front travels through the pinning landscape, while small scales display a balance between thresholds in possible elastic forces and quenched disorder.

1. Introduction

The propagation of cracks in disordered elastic media is a widely studied physical phenomenon, with applications in engineering, and in mechanical hazards in natural media [Bonamy & Bouchaud(2011)]. This fundamental phenomenon rules the failure of man made structures, or of natural materials in Earth science (e.g. [Anderson(1995),Scholz(2002)]). It involves different physical processes, such as long range elastic interactions, thermally activated processes, and heterogeneous material properties.

Modeling of slow crack front propagation at a finite temperature where long range elastic interactions are dominant, is of crucial importance to fill the gap between experiments and models. Experimentally, there has been a number of studies on the advance of crack fronts in mode I, which have shown to present a morphology following scaling laws different at small and large scales [Santucci *et al.*(2010)], an average dynamics compatible with an Arrhenius law [Lengliné *et al.*(2011*b*)], and a velocity distribution displaying a heavy power-law tail $P(v) \sim v^{-2.6}$, [Måløy *et al.*(2006),Tallakstad *et al.*(2011),Santucci *et al.*(2018)], with important consequences for the large scale behavior of the crackling activity [Tallakstad *et al.*(2013)Tallakstad, Toussaint, Santucci & Måløy].

These experimental features are still not reproduced together by a unifying theoretical model, although a number of numerical and theoretical models have been proposed (see review [Bouchaud(1997),Bonamy & Bouchaud(2011)]).

Most of the numerical and theoretical models so far have focused on so-called quasi-static models, defined by force equilibrium, corresponding to a temperature $T = 0$. Some models also consider a rheology with a viscous term linear in velocity [Bonamy & Bouchaud(2011),Patinet *et al.*(2013)]. Such models give rise to an intermittent local activity characterized by a depinning transition and can be viewed as a critical phenomenon [Bonamy & Bouchaud(2011)]. However, these models fail to reproduce experimental conditions as no temperature is introduced in the system. They produce crack velocities limited to a bimodal distribution (either the front is pinned or the front advance is instantaneous), and for most of them, front morphology does not display any cross-over length. These two features are in contradiction with the experimental observations ([Lengliné *et al.*(2011*b*),Santucci *et al.*(2010)]). Quasistatic fiber bundle models have recently been shown to give rise to a cross-over between two scaling regimes ([Gjerden *et al.*(2013)]). Elastic line models have also shown to display two scaling regimes, that can be detected in avalanche distributions or in front morphology, and the cross-over was found to be proportional to the Larkin length ([Laurson *et al.*(2010)]). Some elastic line models with small disorder lead to logarithmic scaling for the front roughness growth ([Ben-Zion & Morrissey(1995)]). However, cracks in both kinds of models are still immobile when under a critical force threshold, unlike experimental ones that show a creep regime. Adding temperature into the system produces a thermal rounding of the depinning transition, allowing movement of the elastic line below the pinning force (e.g. [Bustingorry *et al.*(2008)]). This slow, or creeping regime, has been extensively documented from numerous experiments, notably in the context of rock mechanics (e.g. [Atkinson(1987)]). The mechanism of creep in random environments has also been studied both theoretically and numerically (e.g. [Chauve *et al.*(2000),Chen & Marchetti(1995)]). Creep models often arise as a generalization, at a finite temperature, T, of the models defined in the zero temperature limit. The thermal rounding of the depinning transition however modifies several statistical features compared to extremal models; it notably induces a temperature-dependent correlation length defining scales at which annealed dynamics is dominating [Vandembroucq *et al.*(2004),Bustingorry *et al.*(2008),Kolton *et al.*(2009)]. Little work has however been done on elastic line models at finite temperatures with long range interactions (non local kernel) in heterogeneous media– modelling has been done on the creep of elastic lines following a Paris law, which characterizes the mechanics of fatigue [Lazarus(2011)]. These features of creep of elastic line at finite temperature are of fundamental importance to render the crack propagation under realistic environmental conditions and are necessary for comparisons with experimental

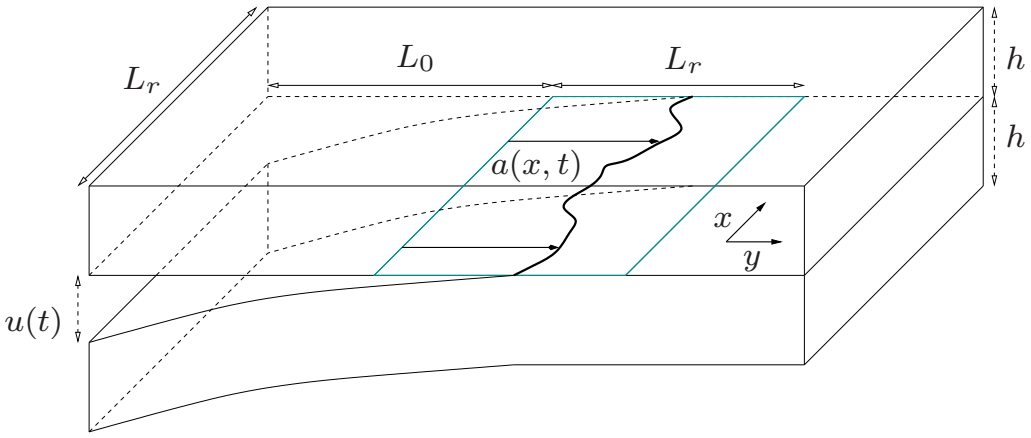

Figure 1. Geometry of the modeled configuration. The square of dimension $L_r \times L_r$ represents the area where we model the crack front propagation.

observations. We propose here a model comprising an annealed noise, represented by an Arrhenius law, quenched disorder, i.e. a random distribution of local toughness, and long-range elastic interactions. Our numerical scheme incorporating these properties differs from those models used to solve similar problems at zero temperature, e.g. the extremal dynamics model [Schmittbuhl *et al.*(1995)] or the BKL algorithm [Rosso & Krauth(2002)].

In order to test the validity of our model, we compare its results with features reported in experiments during interfacial crack propagation. This experimental setup is of particular interest as it has allowed the direct observation of the crack propagation and led to characterization of numerous robust properties of the crack dynamics. We show that our model is in agreement with all reported properties, namely the distribution of the local speeds, the roughness of the crack front line and the macroscopic evolution of the crack. In addition to this numerical model, we also provide theoretical developments, that explain the observed scaling laws, and predict their prefactors and crossover as function of the elastic parameters, quenched disorder distribution, and temperature.

2. Model and Method

We define the modeled interface as a square of dimension $L_r \times L_r$ over which a crack front, $a(x,t)$, is propagating as a function of time t, in the direction y perpendicular to x. We note L_0 the distance between the loading point and the bottom edge of the modeled area. The crack front is thus bounded between L_0 and $L_0 + L_r$. The crack is lying on the middle of two plates of thickness h and width L_r (Fig. 1).

Fluctuations of the fracture energy, $G_c(x,y)$, over the interface are defined on a set of N discrete sites of size $dl = L_r/N$, using a Gaussian distribution of mean μ_{G_c} and standard deviation σ_{G_c} (Fig.2).

The crack front is then loaded by a macroscopic energy release rate, $\bar{G}(t)$, based on the geometry of the experimental setup [Lengliné *et al.*(2011*b*)], assuming a perfectly elastic behavior of the bulk, and neglecting mode II loading [Lengliné *et al.*(2011*a*)]:

$$\bar{G}(t) = \frac{3u(t)^2 E h^3}{8(L_0 + \bar{a}(t))^4}, \tag{2.1}$$

where E is the Young modulus of the plate, h its thickness and $u(t)$ and $\bar{a}(t)$ are the deflection of the beam and the average front position at time t, respectively [Lawn(1993)]. The local fluctuations of the energy release rate along the crack front $a(x,t)$ are expanded from the macroscopic values

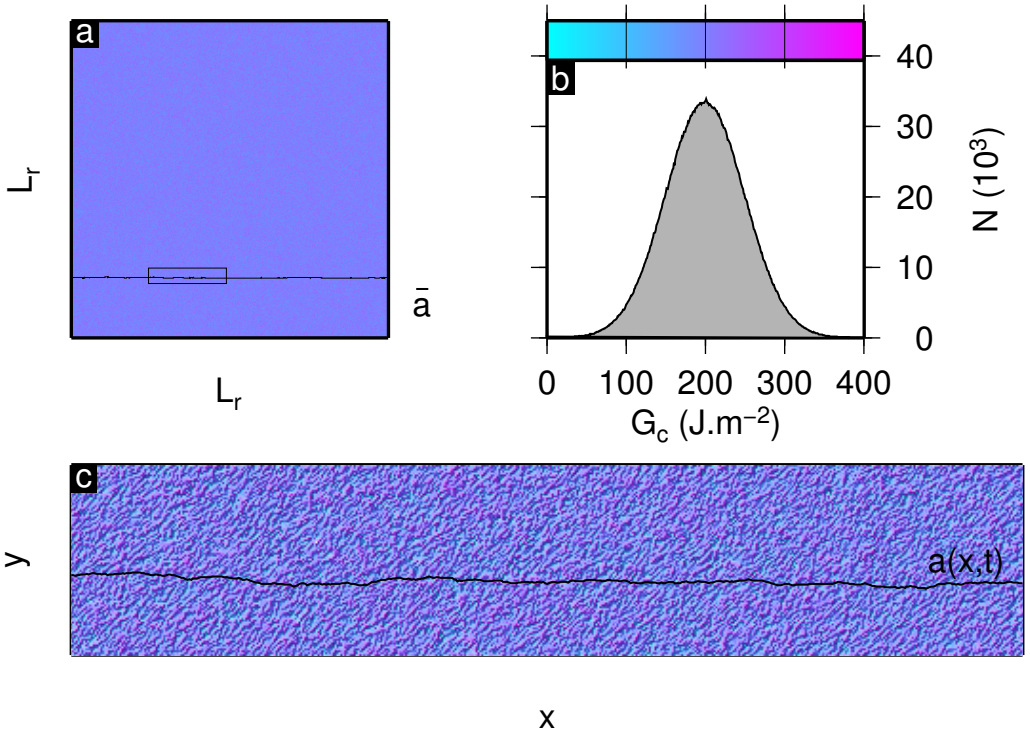

Figure 2. (a) Example of a generated interface with N = 2048. The colors refer to the local values of G_c and the dark line is the crack front line propagating from bottom to top. The average position of the front along the x direction is noted $\bar{a}$. (b) Distribution of the local values of G_c for the surface shown in (a). In this example we set $\mu_{G_c} = 200$ J m^{-2} and $\sigma_{G_c} = 50$ J m^{-2}. (c) Zoom on a sub-part of the interface around the crack front line. The area is represented by a black rectangle in (a).

following [Gao & Rice(1989)]:

$$G[\gamma](x,t) = \bar{G}(t)\,(1+\gamma[a](x,t))\,, \tag{2.2}$$

where $\gamma[a](x,t)$ is the influence function that reflects the static elastic interactions among sites owing to the roughness of the front line:

$$\gamma[a](x,t) = \frac{1}{\pi}\,\mathrm{PV}\int_{-\infty}^{\infty}\frac{a(x',t)-a(x,t)}{(x'-x)^2}dx', \tag{2.3}$$

where PV denotes the principal value.

However Eq. (2.3) is not suitable for numerical implementation, due to the inverse square (hyper) singularity. We also want to use periodic boundary conditions along x to avoid edge effects. Eq. (2.3) may be reformulated using an integration by parts ([Gao & Rice(1989)]) to the weakly singular and more usual expression

$$\gamma[a](x,t) = -\frac{1}{\pi}\,\mathrm{PV}\int_{-\infty}^{+\infty}\frac{\partial a(x',t)/\partial x'}{x-x'}dx'. \tag{2.4}$$

Its corresponding expression for L_r-periodic boundary conditions, obtained after a similar integration by parts, is (simply writing $\int_{-\infty}^{+\infty} = \sum_{n=-\infty}^{+\infty}\int_{n\,L_r}^{(n+1)L_r}$ and assuming $a(x,t)$ is L_r-periodic along x) $\gamma(x,t) = -\frac{1}{L_r}\,\mathrm{PV}\int_0^{L_r}\frac{\partial a(x',t)/\partial x'}{\tan[\pi(x-x')/L_r]}dx'$. However, the spectral formulation introduced by [Perrin *et al.*(1995)], consisting in expressing $a(x,t)$ in (2.4) as a Fourier series of period L_r, is a very natural way of modeling periodic boundary conditions. As a test, we compute

the energy release rate for simple front shapes, expressed from the real space and from the Fourier space formulations, to known analytical solution. We find that this spectral method provides more accurate results than our implementations of the other mathematically equivalent formulations above, so this is what is used for the numerical results shown in this paper.

Specifically, inserting the Fourier series $a(x,t) = \sum_{n=-\infty}^{+\infty} A_n(t) e^{2i\pi nx/L_r}$ in (2.4), and noting that $\mathrm{PV} \int_{-\infty}^{+\infty} \exp(2i\pi nx'/L_r)/(x-x')dx' = -i\pi \mathrm{sign}(n) \exp(2i\pi nx/L_r)$, one gets

$$\begin{aligned}
\gamma[a](x,t) = & \\
& -\frac{1}{\pi} \mathrm{PV} \int_{-\infty}^{+\infty} \frac{(\partial/\partial x')(\sum_{n=-\infty}^{+\infty} A_n(t) e^{2i\pi nx'/L_r})}{x-x'} dx' \\
= & -\frac{1}{\pi} \sum_{n=-\infty}^{+\infty} \mathrm{PV} \int_{-\infty}^{+\infty} \frac{(2i\pi n/L_r) A_n(t) e^{2i\pi nx'/L_r}}{x-x'} dx' \\
= & -\frac{1}{\pi} \sum_{n=-\infty}^{+\infty} (2i\pi n/L_r)(-i\pi \mathrm{sign}(n)) A_n(t) e^{2i\pi nx/L_r} \\
= & -2(\pi/L_r) \sum_{n=-\infty}^{+\infty} |n| A_n(t) e^{2i\pi nx/L_r}
\end{aligned} \tag{2.5}$$

(see also [Cochard & Rice(1997)] section 5). For numerical implementation, the summation is truncated to some large integer, N, and the Fourier coefficients A_n are computed using the same number of sampled values $a_j(t) = a(j \times dl, t)$ through the Discrete Fourier Transform (DFT):

$$\gamma_j(t) = -\sum_{n=-\mathrm{int}((N-1)/2)}^{\mathrm{int}(N/2)} \frac{2\pi|n|}{L_r} \frac{1}{N} \left(\sum_{m=-\mathrm{int}((N-1)/2)}^{\mathrm{int}(N/2)} a_m(t) e^{-\frac{2i\pi nm}{N}} \right) e^{+\frac{2i\pi nj}{N}}, \tag{2.6}$$

remembering that, for N even, the (single) Nyquist component of the DFT, at $j = N/2$, contains information of both the positive and negative Nyquist frequencies: $\mathrm{DFT}[a(t)]_{N/2} = A_{-N/2} + A_{N/2} = 2\Re(A_{N/2}(t))$. In more compact form,

$$\begin{aligned}
\gamma(t) &= \mathrm{DFT}^{-1}[K\, \mathrm{DFT}[a(t)]], \\
K(n) &= -\frac{2\pi|n|}{L_r},
\end{aligned} \tag{2.7}$$

the DFT being evaluated with the FFTW Fast Fourier Transform algorithm [Frigo & Johnson(2005)], keeping in mind that the discrete frequency $n \in [0, N/2]$ for N even and $n \in [0, (N-1)/2]$ for N odd.

We then assume that the propagation of the crack at the local scale (i.e. the mesoscopic scale) is controlled by a process which is defined by an activation energy mechanism. As derived from numerous experiments [Atkinson(1987)] and as verified directly on the considered experimental setup [Lengliné *et al.*(2011*b*)], the advance rate of the crack tip $\dot{a}(x,t)$ is dependent on the temperature T, on the energy release rate G, and on an activation energy which is here assimilated to the fracture energy G_c:

$$\dot{a}(x,t) = v(x,t) = v_1 \, \exp[\lambda \, (G(x,t) - G_c(x,t))], \tag{2.8}$$

with $\lambda = \frac{\alpha^2}{k_B T}$, where α is an atomic length scale associated to the energy barrier of the fracturing process, k_B is the Boltzmann constant and v_1 is related to the velocity for breaking microscopic bonds.

This law arises from basic thermodynamics (see [Lawn(1993)] for kinetic crack growth): for each atomic site undergoing potentially an irreversible breaking transition, there is an activation threshold in free energy $\Delta F_c = F_c - F_0$, below which the material bond only vibrates without breaking - where F_0 is the energy of the non excited unbroken state of this site. This free energy is site dependent, according to the material properties of this bond. Writing it as proportional

to a surface energy, one gets $\Delta F_c = \alpha^2 G_c$, where α is the separation along the surface of the elementary breaking sites. The probability that an energy level F above the basic energy state is reached, is according to statistical physics, a Boltzmannian distribution of the free energy: it is proportional to e^{-F/k_BT}. If the density of energetical states is (roughly) constant – as for example for a quantized harmonic oscillator –, the total probability that the element considered reaches a free energy allowing the breaking transition, above the activation energy ΔF_c, is: $\int_{F>F_c}(e^{-F/k_BT}dF)/\int_{F>F_0}(e^{-F/k_BT}dF) = e^{-\Delta F_c/k_BT}$. If this activation energy is exceeded, the site considered along the front can either break irreversibly, with a transition energy to the next state of basic energy F_1, with a probability proportional to $e^{-(F_1-F)/k_BT}$. It can alternatively unexcite without breaking, and come back to the unbroken state, towards states of basic energy F_0, with a probability proportional to $e^{-(F_0-F)/k_BT}$. The probability that it transitions to a broken state, if the activation energy is reached, is thus $e^{-(F_1-F)/k_BT}/[e^{-(F_0-F)/k_BT} + e^{-(F_1-F)/k_BT}]$ which approximates to $e^{-(F_1-F_0)/k_BT}$, assuming that the broken state is sufficiently energetically favorable compared to thermal noise level, i.e. that $(F_0 - F_1) \ll k_BT$. Since the energy difference between the broken and unbroken states is equal to the mechanical energy release over the surface α^2 along the plane crack covered by the site, one has $(F_0 - F_1) = \alpha^2 G$.

The state of activating and breaking irreversibly the site is thus

$$p_{\text{break}} = e^{-\Delta F_c/k_BT} e^{-(F_1-F_0)/k_BT} = \exp[\alpha^2/(k_BT)\,(G(x,t) - G_c(x,t))].$$

This transition can happen at this basic probability with a characteristic microscopic attempt frequency ν (molecular collisional frequency arising from the characteristics of the phonons in the material, the "thermal bath"), and if the bond irreversibly breaks, the front advances locally by the length α. Hence, with $v_0 = \alpha\nu$, the speed of the front, averaged over a few attempt periods $1/\nu$, is $v = \alpha\nu p_{\text{break}} = v_0 \exp[\alpha^2/(k_BT)\,(G(x,t) - G_c(x,t))]$., which is the Arrhenius law in Eq. 2.8.

We also assume that the temperature is homogeneous and remains constant during the whole crack propagation. This approximation should hold if the temperature variations during the process are smaller than the laboratory absolute temperature, which is around 300 K. For such constant temperature situations, the choice of G_c and v_1 in the rheology, Eq. 2.8, presents a redundancy: any change of these parameters preserving $v_1 \exp([-\lambda G_c(x,t))]$ leads to an identical behavior. In this manuscript, the choice done to raise the invariance under such change is to fix the value of G_c around the characteristic value during the fast stages of the considered situation. In other situations where variable temperatures would be considered, more details on the physico-chemistry of the material would be needed to fix independently G_c and the prefactor v_1.

Once discretized, Eq. (2.8) is in the form of a classical system of N coupled ordinary differential equations (ODE) with time t as the independent variable; it is solved using an 8^{th} order Dormand-Prince Runge-Kutta method as described in [Hairer *et al.*(1993)]. We introduce a flat initial crack front, $a(x, t = 0) = 0$, in the system at time $t = 0$, and $a(x, t)$ is then represented at evenly spaced intervals over L_r along the x axis. As values of $G_c(x, y)$ are only defined at discrete sites, local values of the fracture energy, for arbitrary positions of a along y, are obtained through cubic spline interpolation along y. We tested that different interpolation functions or even no interpolation do not change significantly all the obtained results. We keep a snapshot of the front position every 1 ms in order to mimic what is obtained during experiments with a high speed camera ([Måløy *et al.*(2006)]). A direct visual comparison between crack dynamics shows at first order a good agreement between simulations and experiments (Fig. 3). We recover in the simulation a similar heterogeneous pattern of the front speed which varies of the same order of magnitude in simulations and experiments. In order to draw more quantitative comparisons between our model and experiments we will then examine some well defined properties of the experimental crack fronts.

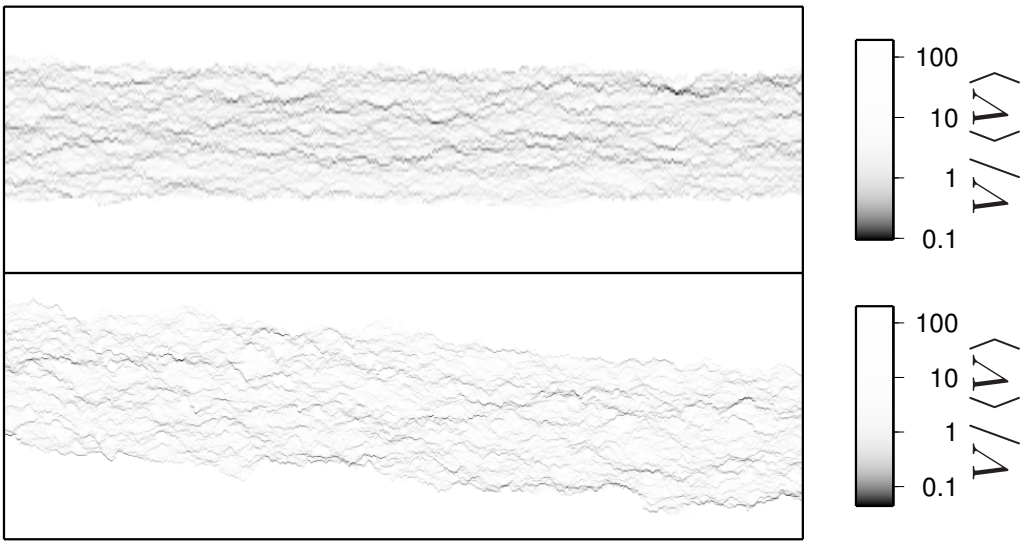

Figure 3. (top) Simulation of a crack front propagation obeying Eq. 2.8. The front propagates from bottom to top, and the displayed interface has a dimension of 5.6 mm along x and 1.4 mm along y. The grayscales refer to the local crack front speed. (bottom) Crack front speed obtained during an experiment from [Tallakstad *et al.*(2011)]. The dimension of the interface are identical to (top).

3. Macroscopic crack evolution

We aim at testing the validity of our model by comparing its predictions with several independent experimental behaviors. We first set several *a priori* parameters of the model in order to match the experimental setting. Young modulus is set to $E = 3.2$ GPa. Geometrical parameters are defined as: $h = 5$ mm, $L_r = 2.84$ cm, for the plate thickness and width, respectively. We set $N = 2048$. The average fracture energy is $\mu_{G_c} = 200\,\mathrm{J\,m^{-2}}$ as a representative value of the experiments [Lengliné *et al.*(2011*b*)]. We invert for the values of v_1 and λ from the macroscopic behavior of the crack front by comparing the results of simulations with an experiment reported in [Lengliné *et al.*(2011*a*)] with two loading phases: Phase I at a constant loading speed $V_l = \dot{u}(t) = 62\,\mu\mathrm{m\,s^{-1}}$ for 230 s, and phase II for which the deflection of the beam is maintained constant. The initial front position is $L_0 = 107.7$ mm. We checked that higher values of N induce no change in the macroscopic evolution of the crack. Experimental data are well reproduced by the model when setting $\lambda = 0.15\,\mathrm{m^2\,J^{-1}}$ and $v_1 = 0.031\,\mathrm{m\,s^{-1}}$ (Fig. 4). This suggests that the Arrhenius law remains valid on a scale larger than the one at which it was set in the model [Lengliné *et al.*(2011*b*)]. It should also be noted that the value of λ corresponds to the value inferred experimentally by [Lengliné *et al.*(2011*b*)], who found $\lambda = 0.15\,\mathrm{m^2 J^{-1}}$, averaging over multiple experiments. The average velocity along the front v as function of the average energy release rate $\bar{G}$, shown in Fig. 4 right, was computed using the same technique as the experiments, using the velocity derived via the WTM (Waiting Time Matrix) at a similar pixel scale (as in Fig. 3). This Waiting Time Matrix analysis is based on the following: on a discrete regular grid, W_{ij} is defined as the number of times a front is observed to cross this given pixel ij during an experiment. The front velocity while the front was at this position is then obtained as $v_{ij} = \Delta x/(\Delta t W_{ij})$, where Δx is the spatial lattice step, and Δt the interval between two subsequent front positions (the frame rate in the experiments or the simulations). Alternatively, using instead directly the instantaneous velocities computed leads to a more disperse average velocity as function of $\bar{G}$, with the same average value at a given $\bar{G}$. This instantaneous front velocity reduces to a similar behavior as the one obtained via the WTM when this velocity is averaged over time windows of 0.03 s or larger.

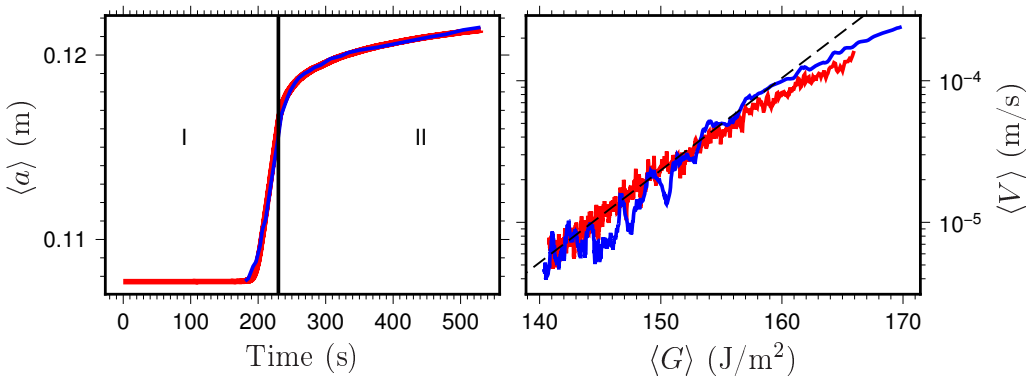

Figure 4. Left: Evolution of the crack front position during an experiment (blue line from [Lengliné *et al.*(2011*b*)]) and from the simulation (red line) using $\lambda = 0.15$ m^2 J^{-1} and $v_1 = 0.031$ m s^{-1}. The vertical black line separates phase I at constant loading rate and phase II, the relaxation phase. Right: Evolution of average crack speed $\bar{v}$ as a function of the energy release rate $\bar{G}$ for the experimental data (blue dots) and for the simulation (red dots). The dashed line shows that a fit of the form of Eq. (2.8) with $\lambda = 0.15$ m^2 J^{-1} and $v_1' = 0.013$ m s^{-1}. v_1' is slightly lower than v_1 (the difference between v_1 and v_1' decreases slowly with σ_{G_c} here taken as $\sigma_{G_c} = 50$ J m^{-2}).

4. Distribution of local speeds

At the local scale, we evaluate the distribution of the crack front speeds in our model. As reported in [Måløy *et al.*(2006),Tallakstad *et al.*(2011),Lengliné *et al.*(2011*b*)], the distribution of local speeds higher than the average crack front velocity is found to decay as a power law with exponent $\eta = -2.55$. We selected a period when the average speed of the crack is approximately constant and computed the local speed distribution similarly to the procedure introduced by [Måløy *et al.*(2006)]. Exploring the parameter space, we observed that the simulated distributions are controlled by the parameter $(\sigma_{G_c}/\mu_{G_c})^2\lambda = 1/\rho$ (as illustrated in Fig. 5 where several toughness distributions produce the same velocity distribution). Moreover, N does not have a significant influence on the value of η. For $\rho \simeq 125$ J m^{-2}, we find that the power law decay of the distribution at high velocities exhibits a slope compatible with the experimental observations, i.e., $\eta = -2.55$. Given the value of $\lambda = 0.15$ m^2 J^{-1} as deduced from the macroscopic evolution of the crack we then deduce $\sigma_{G_c} = 50$ J m^{-2} for $\mu_{G_c} = 192$ J m^{-2}. It is worth mentioning that the standard deviation $\sigma_{G_c} = 50$ J m^{-2} matches the one observed experimentally [Lengliné *et al.*(2011*b*)]. At higher values of ρ, i.e. lower quenched disorder, the logarithm of the probability distribution function is closer to a quadratic function of $\log(v)$ around its maximum, i.e. the distribution is close to lognormal - see insert of Fig. 5, $\rho = 500 J/m^2$. When the quenched disorder is large enough, a power law tail at high velocities is observed over around two decades for the distribution of velocities, the observed exponent is in the range η between 2.2 and 3 for the probed values of ρ.

5. Front morphology

We also investigated the scaling of the crack front morphology. Previous experimental studies reported that the crack front is self-affine with a roughness exponent $\zeta \simeq 0.6$ (e.g. [Schmittbuhl & Måløy(1997),Delaplace *et al.*(1999)]). More recent data extracted from numerous experiments and at various scales show that actually two distinct regimes emerge depending on the scale of investigation: at small scales the scaling regime is characterized by a roughness exponent $\zeta^- \simeq 0.60$ while at large scale the exponent is lower and is found around $\zeta^+ \simeq 0.35$ [Santucci *et al.*(2010)]. From simulations at constant loading velocity, we first investigate the scaling of energy release rate profiles, $G(x)$, before turning to the scaling of $a(x)$. These profiles correspond

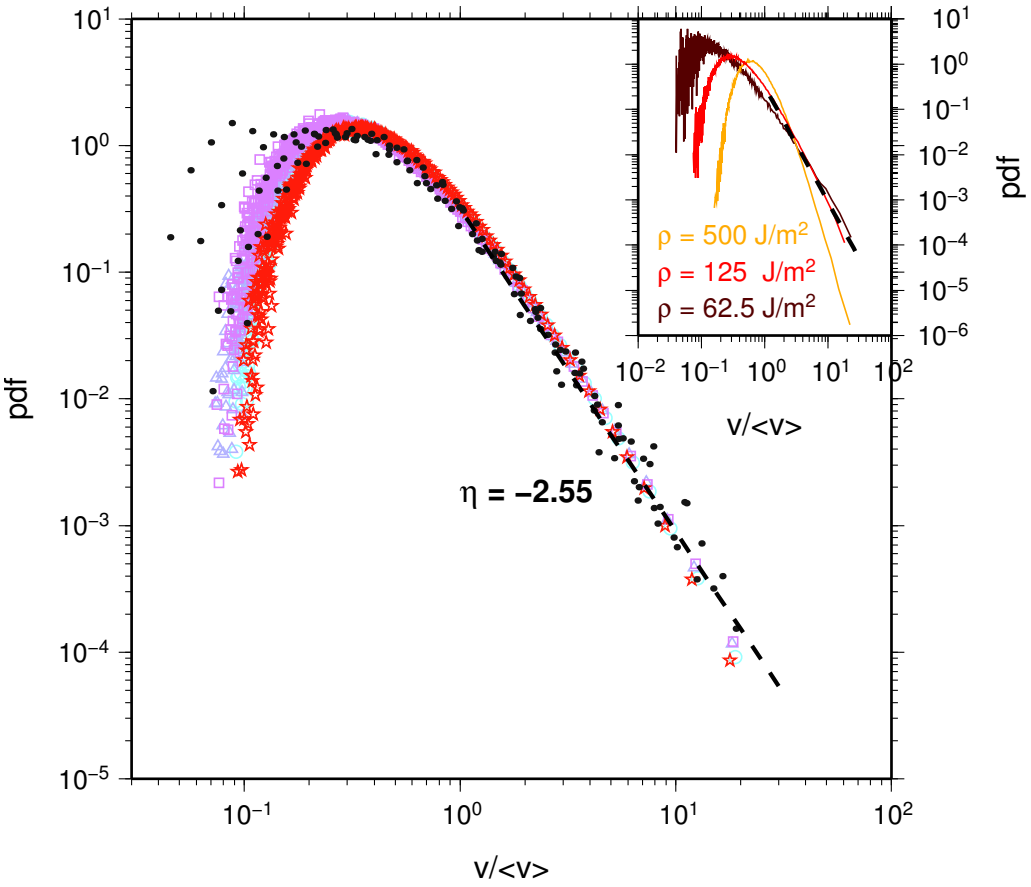

Figure 5. Probability density functions (pdf) of the local crack velocity computed from simulations. Local crack velocity is normalized for each simulation by the average crack front velocity $\langle v \rangle$. Collapse of four distributions for the same $\rho \simeq 125$ J/m^2 ($\triangle$: $\lambda = 0.13$, $\mu_{G_c} = 200$, $\sigma_{G_c} = 50$; $\circ$: $\lambda = 0.2$, $\mu_{G_c} = 200$, $\sigma_{G_c} = 40$; $\square$: $\lambda = 0.08$, $\mu_{G_c} = 200$, $\sigma_{G_c} = 63$; $\star$: $\lambda = 0.13$, $\mu_{G_c} = 160$, $\sigma_{G_c} = 40$). Black dots correspond to experimentally obtained speed distributions taken from [Tallakstad *et al.*(2011)]. A power law with an exponent $\eta = -2.55$ (dashed line) is consistent with the pdf tail for $v/\langle v \rangle > 1$ as observed experimentally [Måløy *et al.*(2006)]. Insert: pdfs for two other values of ρ: 500 J/m^2 and 62.5 J/m^2.

to the local values of energy release rate for all points on the crack front. We compute the scaling properties of the crack energy release rate profile after averaging 1000 power spectra evenly time-spaced (after a transient regime from an initial condition of flat front). The crack energy release rate along the front is defined as $G(x,t) = G(x, a(x,t))$, expressed from Eq. (2.2) along the modeled fronts of shape $a(x,t)$. We first look at its spatial Fourier power spectrum, $P_G(k)$ for a simulation running with parameters deduced from previous tests, namely we use $\lambda = 0.13$ m^{2}J^{-1}, $\mu_{G_c} = 200$ J/m^2 and $\sigma_{G_c} = 50$ J/m^2. We see in Fig. 6 that $P_G(k)$ becomes flat in the high wavenumber domain, reaching the value $\sigma^2_{G_c}$. This upper limit corresponds to the expected power spectrum of a straight 1D line cut through the $G_c(x,y)$ field. It suggests that, at small scales, fluctuations of energy along the crack front line follow the quenched disorder variations, with a power spectrum insensitive to the deviations between the curved front and a straight line at the average front position. For lower wavenumbers, $P_G(k)$ deviates from the constant threshold and becomes a growing function of k (decreasing as k diminishes, as seen in Fig. 6). We can well render the evolution of $P_G(k)$ at these large scales with a relation of the form $P_G(k) \propto k$.

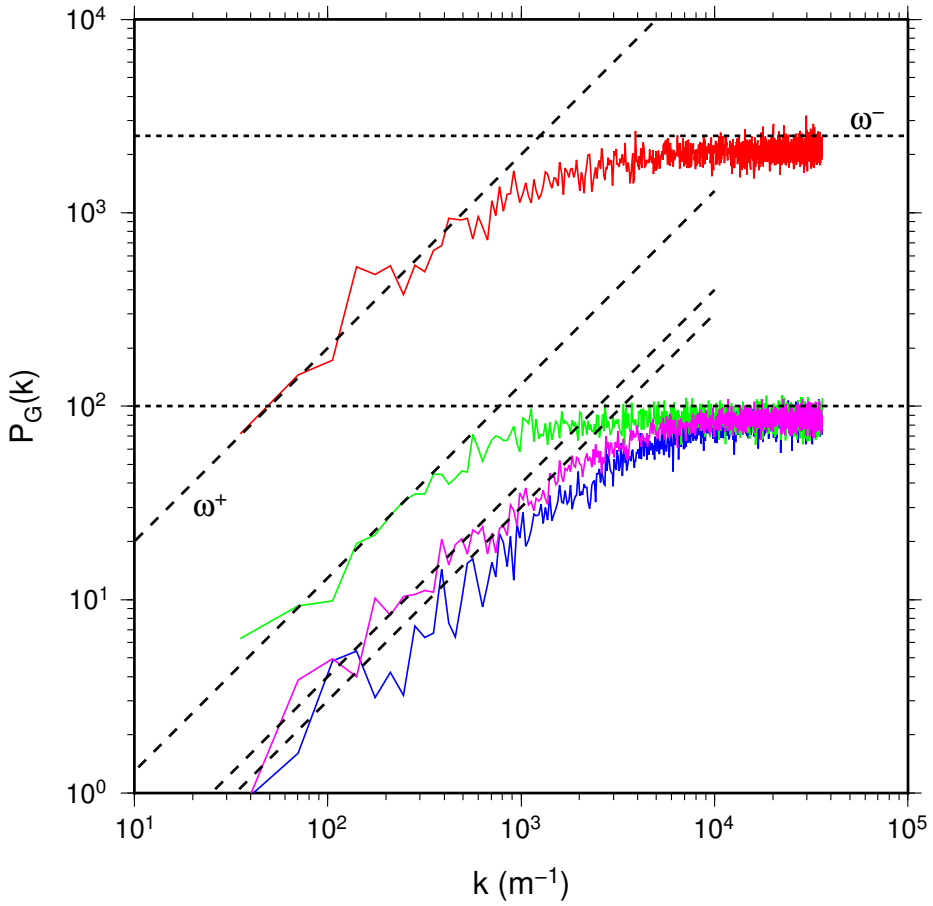

Figure 6. Power spectra of the energy release rate, $P_G(k)$, computed for different simulations. The spectrum in red is computed for a simulation with $\lambda = 0.13$ m^{2}J^{-1}, $\mu_{G_c} = 200$ J/m^2 and $\sigma_{G_c} = 50$ J/m^2. For the other spectra: $\sigma_{G_c} = 10$ J/m^2 and $\lambda = 0.21$ m$^2/J$ for the spectrum in green and $\lambda = 0.05$ m^{2}J^{-1} for the one in blue; for the spectrum in magenta, we keep $\lambda = 0.13$ m^{2}J^{-1} but change μ_{G_c} to 100 J/m^2. The horizontal dashed lines correspond to $\sigma^2_{G_c}$ while the slanted dashed lines are given by $P_G(k) \propto C\lambda\sigma^2_{G_c}\mu_{G_c}k$. We note ω^+ and ω^- the pre-factor of $P_G(k)$ at large scale and the level of $P_G(k)$ at small scale, respectively.

We also report in Fig. 6 several simulations where the parameters, λ, μ_{G_c} and σ_{G_c} were modified in order to test their influence on the spectrum of the energy profile. For all simulations we always observe the threshold at high wavenumbers corresponding to $\sigma^2_{G_c}$ and also evidenced $P_G(k) \propto k$ at low k. We can evaluate from the tested parameters that at low k, $P_G(k) \propto C\lambda\sigma^2_{G_c}\mu_{G_c}k$, with C a constant – as seen from the consistency of the simulation data and the dotted lines in Fig. 6. By equating the power-spectra in the two spatial frequency domains, we infer the cross-over, k_δ, above which the energy of the front line follows the energy profile of the medium. We obtain $k_\delta = 1/(\lambda\mu_{G_c}C)$, which implies that the cross-over is independent of the amplitude of the quenched disorder fluctuations, σ_{G_c}, but varies with the temperature and the mean toughness of the interface, μ_{G_c}.

We can now turn to the scaling of the front position. As indicated from Eq. 2.6, the scaling of a is related to the scaling of G. Indeed, from Eq. 2.7 we have

$$\mathrm{DFT}[\gamma(t)](n) = K(n)\,\mathrm{DFT}[a(t)](n), \tag{5.1}$$

with $K(n) = -2\pi|n|/L_r$, and the equivalent formulation in the continuous domain, since the wavenumber n is related to the wavevector k as $k_n = 2\pi n/L_r$, is given by

$$\tilde{\gamma}_k = -|k|\tilde{a}_k. \tag{5.2}$$

where the tilde denotes the Fourier transform defined as $\tilde{f}(k) = \int f(x)e^{-ikx}dx$.

Expressing in the Fourier space the link between the energy release rate G and the elastic Kernel γ, reminding Eq. 2.2, we get for any non zero wavevector k,

$$\tilde{G}(k,t) = \bar{G}(t)\tilde{\gamma}(k), \tag{5.3}$$

since the additive constant term in Eq. 2.2 only contributes to the $k=0$ mode, and the multiplicative prefactor $=\bar{G}(t)$ is independent of position.

We thus expect from these last two equalities, for the power spectra $P_a(k)$ and $P_G(k)$ of the front shape $a(x)$ and of the energy release rate $G(x)$:

$$P_a(k) = ||\tilde{a}_k||^2 = ||\tilde{\gamma}_k||^2/k^2 \propto P_G(k)k^{-2} \tag{5.4}$$

which, given the observed scaling of $P_G(k)$, translates into

$$\begin{aligned} P_a(k) &\propto k^{-1} \quad \text{for} \quad k < k_\delta \qquad \text{and} \\ P_a(k) &\propto k^{-2} \quad \text{for} \quad k > k_\delta. \end{aligned} \tag{5.5}$$

We indeed observe the aforementioned crack front morphology in our numerical simulations (Fig. 7), i.e. we obtain the two regimes discussed above. At long wavelengths, the observed roughness exponent is $\zeta^+ \simeq 0.0$ while, at shorter length scales, ζ^- is 0.5. This is compatible with the experimental observations [Santucci *et al.*(2010)], where at short length scales, $\zeta^- \simeq 0.5$ is determined, while at larger scales, a flattening to lower exponents is observed – which is compatible with local exponent $\zeta^+ \simeq 0.3$ to 0.4, and also compatible with a slow cross over towards a flattening $\zeta^+ \simeq 0$ (which corresponds to a subpower law scaling law, as a logarithmic behavior $|a(x+\Delta x) - a(x)| \sim \log(|\Delta x|)$. (This reference mentioned: "At large scales, we observe a crossover to another scaling regime with a smaller roughness exponent $\zeta = 0.35 \pm 0.05$. Our data do not rule out a possible slow crossover to a flat front (no disorder regime), at large scales"). Indeed, in the simulation a local $\zeta^+ \simeq 0.35$ is compatible with the results over one to two decades of cross over, as illustrates the compatibility with the dash dotted line in Fig. 7 around the cross-over scales, and as observed in the experiments [Santucci *et al.*(2010)].

In order to show the influence of temperature on the variation of k_δ we show the averaged power spectra for different temperatures (i.e. different λ) which can be nicely superimposed by introducing a normalized wavenumber $k^* = k/k^{\text{ref}}(T^{\text{ref}}/T)$ where T^{ref} is a reference temperature and k^{ref} a reference wavenumber (see Fig. 7). As will be shown in Section 6, the constant $(T^{\text{ref}}/k^{\text{ref}})$ depends on the correlation length l_c of the quenched disorder, i.e. the critical energy release rate G_c, and its average value μ_{G_c}, as $T^{\text{ref}}f/k^{\text{ref}} = \alpha^2 l_c \mu_{G_c}/(2k_B)$.

Interestingly, the cross-over $R_c = 1/k_\delta$ between the two domains can be estimated for $\lambda = 0.13\ \text{m}^2\ \text{J}^{-1}$ and $\mu_{G_c} = 200\ \text{J/m}^2$ to be $\sim$ 1 mm, which is comparable to the value reported experimentally [Santucci *et al.*(2010)]. The observed dependence of the cross-over length on temperature has been previously noticed for different models. In the case of short range elastic interactions, it is found that R_c varies with T with a power-law exponent depending on the percolation properties of the active sites [Vandembroucq *et al.*(2004)]. Other studies proposed that the cross-over length scale might also depend on the difference between the driving force and the depinning threshold (e.g. [Chauve *et al.*(2000),Kolton *et al.*(2009)]). We also observe that changing the cut-off wavelength of the toughness correlation, l_c, influences the cross-over scale R_c, which can be seen as a temperature effect.

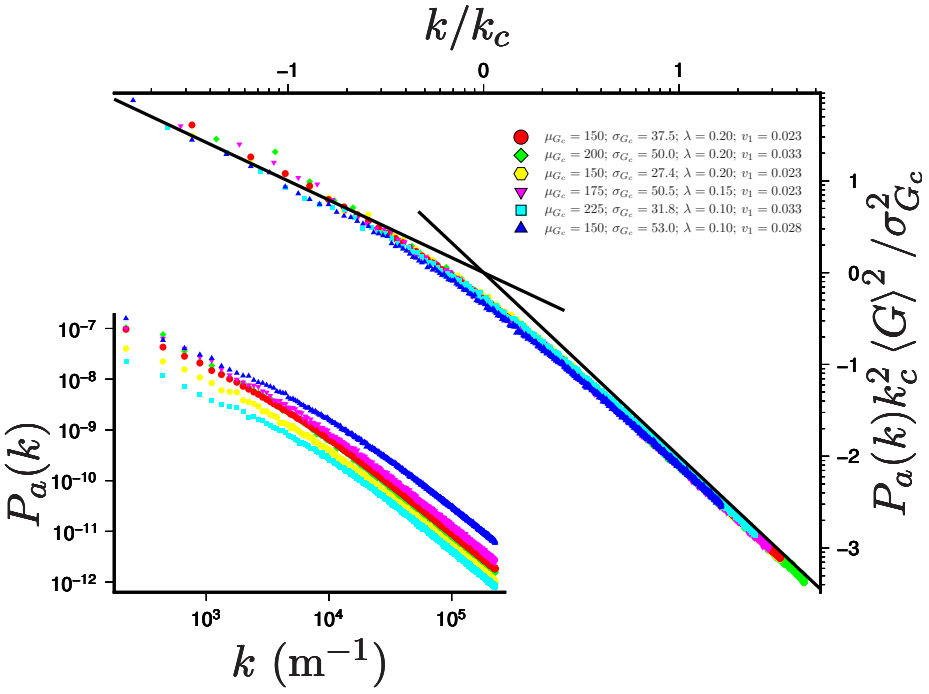

Figure 7. (Insert) Average power spectrum ($P_a(k)$) computed over 1000 crack fronts during simulations when varying $\lambda = \alpha^2/k_BT$. Units of the parameters in the legend are for G_c, Jm^{-2}, for λ, m^2/J and for v_1, m/s. (Main) Collapse of all power spectra at different temperatures after rescaling the wavenumber $k^* = k/k_c = (k/k^{\text{ref}})(T^{\text{ref}}/T)$., and the norm according to the predicted prefactor. The two power-laws corresponding to the continuous curve have slopes -1 and -2, i.e. correspond to Hurst exponents $\zeta^+ = 0$ at large scales (small k, logarithmic scaling), and $\zeta^+ = 0.5$ at small scales (large k).

6. Theoretical interpretation of the dominant forces at large and small scales

The dynamics of the crack front, at finite temperature, is led by the Arrhenius law from Eq. (2.8), with the energy release rate by Eq. (2.2) as the product of the average value $\bar{G}$ from Eq. (2.1), and the elastic perturbation $\gamma(a)$, that depends on the shape of the front $a(x)$ as stated by Eq. (2.3):

$$\dot{a}(x,t) = v_1 \exp[\lambda\,(G(x,t) - G_c(x,t))], \tag{6.1}$$

$$G[a](x,t) = \bar{G}(\bar{a},u)(1+\gamma[a]). \tag{6.2}$$

The quenched disorder associated to the material properties corresponds to a spatial distribution of the critical energy release rate:

$$G_c(x,t) = G_c(x,a(t)) = \bar{G}_c + \delta G_c(x,a(t)). \tag{6.3}$$

Inserting Eq. (6.2) and Eq. (6.3) into Eq. (6.1) leads to

$$\dot{a}(x,t) = v_1 \exp\left[\lambda\left(\bar{G} + \bar{G}\gamma[a] - \bar{G}_c - \delta G_c(x,a(t))\right)\right]. \tag{6.4}$$

Assuming that the average critical energy release rate along the front during propagation is around the average value of the quenched distribution in the plane, $\bar{G}_c \sim \mu_{G_c}$, we can write

$$\dot{a}(x,t) = \bar{v} \exp[\lambda\left(\bar{G}\gamma[a] - \delta G_c(x,a(t))\right)], \tag{6.5}$$

where

$$\bar{v} \simeq v_1 \, \exp\left[\lambda\left(\bar{G} - \mu_{G_c}\right)\right]. \tag{6.6}$$

This last equation can be expressed with a one dimensional Fourier transform as

$$\dot{a}(x,t) = \sum_k \dot{\tilde{a}}_k e^{ikx} = \tag{6.7}$$

$$\bar{v} \, \exp\left[\sum_{k\neq 0} \lambda\bar{G} e^{ikx}\left(\tilde{\gamma}_k(t) - \delta\tilde{G}_{ck}(t)/\bar{G}\right)\right] =$$

$$\bar{v} \, \Pi_{k\neq 0} \exp\left[\lambda\bar{G} e^{ikx}\left(\tilde{\gamma}_k - \delta\tilde{G}_{ck}/\bar{G}\right)\right]. \tag{6.8}$$

The product above can be considered as follows: each of the product terms have a form

$$\exp\left[\lambda\bar{G}\Re\left[e^{ikx}\left(\tilde{\gamma}_k - \delta\tilde{G}_{ck}/\bar{G}\right)\right]\right] \cdot$$

$$\exp\left[\lambda\bar{G} i \Im\left[e^{ikx}\left(\tilde{\gamma}_k - \delta\tilde{G}_{ck}/\bar{G}\right),\right]\right] \tag{6.9}$$

where $\Re(z)$ and $\Im(z)$ refer respectively to the real and imaginary parts of the complex number z. The second term in the product is the exponential of a pure imaginary number, of norm 1: it does not affect the norm of the product. The first term in the product can be written as

$$\exp\left[\lambda\bar{G}\Re\left[e^{ikx}\left(\tilde{\gamma}_k - \delta\tilde{G}_{ck}/\bar{G}\right)\right]\right]$$

$$= \quad \exp\left[\Re\left(||z|| e^{i\theta} e^{ikx}\right)\right] \tag{6.10}$$

$$= \quad \exp\left[||z|| \cos(\theta + kx)\right], \tag{6.11}$$

$$\text{where} \quad z = \lambda\bar{G}\left(\tilde{\gamma}_k - \delta\tilde{G}_{ck}/\bar{G}\right)$$

$$\text{and} \quad \theta = arg(z)$$

For any k, there are positions $x \simeq -\theta[2\pi]/k$ where the product above reduces to $\exp\left[||z||\right]$.

Hence, if the norm $||z||$ is not significantly smaller than 1, then for certain positions x, the value of the term in the product, $\exp(||z||)$, becomes exponentially large, so that the front speed will become locally large, and the unpinned front shuffles very fast, during an avalanche, through new configurations of the quenched disorder – until this term $||z||$ becomes small again for all k.

Three cases can be considered to obtain the value of $||z|| = ||\lambda\bar{G}\left(\tilde{\gamma}_k - \delta\tilde{G}_{ck}/\bar{G}\right)||$:

if $||\tilde{\gamma}_k|| \ll ||\delta\tilde{G}_{ck}/\bar{G}||$, this term can be approximated as $||z|| \simeq ||\lambda\delta\tilde{G}_{ck}||$, and z is given by $z \simeq -\lambda\delta\tilde{G}_{ck}$. The magnitude of this is of order $\lambda\sigma_{Gc}$, which is smaller than one, allowing to approximate $\exp(z) \sim 1 + z$. When $||\tilde{\gamma}_k|| \simeq ||\delta\tilde{G}_{ck}/\bar{G}||$, the order of magnitude of z is also $||z|| \leq \lambda\sigma_{Gc}$, smaller than one. Eventually, if $||\tilde{\gamma}_k|| \gg ||\delta\tilde{G}_{ck}/\bar{G}|| \simeq \sigma_{Gc}/\bar{G}$, one has $||z|| \simeq ||\lambda\bar{G}\tilde{\gamma}_k|| \gg \lambda\sigma_{Gc}$. Since $\lambda\sigma_{Gc}$ is a finite number (around 0.1 to 1 in the simulation examples, that correspond to the experimental match), this case where $||z|| \gg \lambda\sigma_{Gc}$ also corresponds to $||z|| \gg 1$, which is discussed in the previous paragraph: this situation is unstable and corresponds to a large velocity, an avalanche during a depinning event.

The product of all these exponential terms, in a configuration where they are stabilized in situations where $||\tilde{\gamma}_k|| \simeq ||\delta\tilde{G}_{ck}/\bar{G}||$, will be denoted $R(t)$, and apart from the fast avalanches, it will stay constant, around 1.

Conversely, for other values of k, the perturbation due to the elastic interactions will always be small in front of the quenched disorder, i.e., at all times, we will have

$$||\tilde{\gamma}_k|| \ll ||\delta\tilde{G}_{ck}/\bar{G}||, \tag{6.12}$$

so that for all positions x, at all times, we will have

$$||\lambda\bar{G}\Re\left[e^{ikx}\left(\tilde{\gamma}_k - \delta\tilde{G}_{ck}/\bar{G}\right)\right]|| \ll 1. \tag{6.13}$$

For these modes, with $\epsilon_k = \lambda \bar{G} e^{ikx} \left(\tilde{\gamma}_k - \delta \tilde{G}_{ck}/\bar{G} \right)$, and $||\epsilon_k|| \ll 1$, the exponential terms in the sum can be approximated as $\exp(\epsilon_k) \simeq 1 + \epsilon_k$, and the product, to leading order, as

$$\Pi_k(\exp(\epsilon_k)) \simeq \Pi_k(1 + \epsilon_k) \simeq 1 + \Sigma_k \epsilon_k. \tag{6.14}$$

For these modes, there will be constantly slow accelerations or decelerations around an average rate of change.

With these considerations over the two types of modes, the sum over non zero wavenumbers can thus be approximated as follows in Eq. (6.8): large terms are unstable in this sum, since the velocity depends exponentially on the sum, and the sum blows up quickly when a term grows above the average. When the terms of the sum are small with respect to 1, they modulate the velocity with respect to the average velocity. We conclude that there are two possible cases for the interaction term: either it is small enough so that

$$||\tilde{\gamma}_k|| \ll ||\delta \tilde{G}_{ck}||/\bar{G}, \tag{6.15}$$

or, after a very short time, the Fourier component jumps to a new value where it is comparable to the average velocity. Apart from the very short unstable times where the velocity jumps far from the average, the Fourier modes take random values within the characteristic value:

$$||\tilde{\gamma}_k|| \sim ||\delta \tilde{G}_{ck}||/\bar{G}. \tag{6.16}$$

Considering the case where interactions are small, the velocity, from Eq. (6.8), can thus be expressed as

$$\dot{a}(x,t) = \sum_k \dot{\tilde{a}}_k e^{ikx} = \bar{v} R(t) \times \tag{6.17}$$

$$\exp \left[\sum_{k \neq 0; ||\tilde{\gamma}_k|| \ll ||\delta \tilde{G}_{ck}/\bar{G}||} \lambda \bar{G} e^{ikx} \left(\tilde{\gamma}_k - \delta \tilde{G}_{ck}/\bar{G} \right) \right]$$

where the sum is limited over wavenumbers that produce a stable propagation of the front. $R(t)$ is the fluctuating term taking into account the jumps to bring back the argument of the exponential to the average value by reshuffling the values of $\tilde{\gamma}_k$ that go for short periods beyond the saturation level: it is most of the time around 1, with these short periods of large values above it – intermittent avalanches.

As introduced above, in the other case for the interaction term, we have a saturation so that $||\tilde{\gamma}_k|| \sim ||\delta \tilde{G}_{ck}||/\bar{G}$. We first focus on this case, which defines the range where elastic interactions are balancing quenched noise amplitude. The level of saturation is set by the amplitude of the quenched disorder fluctuations with respect to the average. Indeed, the power spectrum, $P_G(k)$, is given by Eq. (6.2), valid for any $k \neq 0$:

$$P_G(k) = \bar{G}^2 ||\tilde{\gamma}_k||^2. \tag{6.18}$$

Since, in the considered case

$$||\tilde{\gamma}_k|| \sim ||\delta \tilde{G}_{ck}||/\bar{G}, \tag{6.19}$$

we can write

$$P_G(k) = ||\delta \tilde{G}_{ck}||^2 \tag{6.20}$$

and as $||\delta \tilde{G}_{ck}|| \sim \sigma_{G_c}$, for non correlated quenched noise, the power spectrum $P_G(k)$ scales as

$$P_G(k) \sim \sigma^2_{G_c}.$$

This theoretical prediction is satisfied, as shown by the various levels of dashed lines at large wavenumbers in Fig. 6. This behavior of saturation of the interaction kernel at large k, i.e. at small scales, is identical to the one expected in a quasi-static model, in which the elastic kernel exactly balances the quenched disorder. Hence, this model at finite temperature predicts, at small scale,

front morphologies comparable to those expected in such models [Schmittbuhl & Vilotte(1999), Favier *et al.*(2006),Pindra *et al.*(2009)].

Hence, at small scale, the amplitude of the Fourier mode of the elastic kernel saturates around a characteristic amplitude. This has a direct consequence on the front morphology: this elastic kernel can also be expressed as function of the front shape, which in Fourier space reads from Eq. (5.2) as

$$||\tilde{\gamma}_k|| \sim |k|\,||\tilde{a}_k|| \tag{6.21}$$

Since, from Eq. 6.20, $||\tilde{\gamma}_k|| \sim |k| \sim ||\delta\tilde{G}_{ck}||/\bar{G}$, this implys for the Fourier amplitude of the front shape $\tilde{a}_k$, at these scales, that

$$|k|\,||\tilde{a}_k|| \sim ||\tilde{\gamma}_k|| \sim ||\delta\tilde{G}_{ck}||/\bar{G}, \tag{6.22}$$

i.e.

$$||\tilde{a}_k|| \sim ||\delta\tilde{G}_{ck}||/|k|\bar{G}, \tag{6.23}$$

or, for non correlated quenched noise, since $||\delta\tilde{G}_{ck}|| \sim \sigma_{G_c}$, one expects a power spectrum of the front as

$$P_a(k) = ||\tilde{a}_k||^2 \sim \sigma^2_{G_c}/k^2 = \sigma^2_{G_c} k^{-1-2\cdot\zeta}, \tag{6.24}$$

i.e. a self affine scaling [Santucci *et al.*(2010)] with a Hurst exponent ζ such that $-2 = -1 - 2\zeta$, i.e. $\zeta = 0.5$.

On the contrary, for the other case, $||\tilde{\gamma}_k|| \ll ||\delta\tilde{G}_{ck}||/\bar{G}$, i.e. elastic interactions are well below the quenched noise amplitude. Using this, one can linearize Eq. (6.17), leading to

$$\begin{aligned} \dot{a}(x,t) \quad &\simeq \quad \bar{v}R(t) + \lambda\bar{G}\bar{v}R(t) \times \\ &\sum_{k\neq 0;||\tilde{\gamma}_k|| \ll ||\delta\tilde{G}_{ck}/\bar{G}||} e^{ikx}\left(\tilde{\gamma}_k - \delta\tilde{G}_{ck}/\bar{G}\right), \end{aligned} \tag{6.25}$$

which describes the evolution of the crack front line when interactions are small. It will be shown later that this behavior is observed at large wavelength, i.e. small wavenumber. For this domain, one has, as shown above, using the average value $R(t) \sim 1$ as an approximation for $R(t)$, which is most of the time around such value:

$$\begin{aligned} \dot{\tilde{a}}_k(t) \quad &\simeq \quad \lambda\bar{v}\left(\bar{G}\tilde{\gamma}_k - \delta\tilde{G}_{ck}\right) \\ &\simeq \quad \lambda\bar{v}\left(-\bar{G}|k|\tilde{a}_k - \delta\tilde{G}_{ck}\right). \end{aligned} \tag{6.26}$$

This ordinary differential equation can be integrated in time, noting that:

$$\frac{d}{dt}\left(\tilde{a}_k(t)e^{\lambda\bar{v}\bar{G}|k|t}\right) \quad = \quad \left(\dot{\tilde{a}}_k(t) + \lambda\bar{v}\bar{G}|k|\tilde{a}_k\right)e^{\lambda\bar{v}\bar{G}|k|t} \tag{6.27}$$

$$\simeq \quad -\lambda\bar{v}\delta\tilde{G}_{ck}e^{\lambda\bar{v}\bar{G}|k|t}, \tag{6.28}$$

so that, by the variable constant method,

$$\begin{aligned} &\tilde{a}_k(t)e^{\lambda\bar{v}\bar{G}|k|t} = \\ &\tilde{a}_k(t=0) - \int_0^t dt'\lambda\bar{v}\delta\tilde{G}_{ck}(t')e^{\lambda\bar{v}\bar{G}|k|t'} \end{aligned} \tag{6.29}$$

and the solution can be expressed as:

$$\begin{aligned} &\tilde{a}_k(t) = \\ &-\int_0^t dt'\lambda\bar{v}\delta\tilde{G}_{ck}(t')e^{\lambda\bar{v}\bar{G}|k|(t'-t)} + \tilde{a}_k(t=0)e^{-\lambda\bar{v}\bar{G}|k|t}. \end{aligned} \tag{6.30}$$

The process is thus similar to an anomalous diffusion with a random term arising from the quenched disorder through which the system goes at average speed, $\lambda\bar{v}\delta\tilde{G}_{ck}(t')$. Such anomalous diffusion systems are common in systems with interactions, e.g. in fluctuating dipolar chains

[Toussaint *et al.*(2004),Toussaint *et al.*(2006)]. The first term represents the convolution of the random term due to the material variable properties by the response function representing the memory of the system, $e^{-\lambda\bar{v}\bar{G}|k|t}$. The second term represents the memory of the initial conditions. For initially straight fronts, it is equal to zero. For large enough propagation times, one can also write:

$$\tilde{a}_k(t) = -\int_{-\infty}^{t} dt' \lambda\bar{v}\delta\tilde{G}_{ck}(t')e^{\lambda\bar{v}\bar{G}|k|(t'-t)}. \tag{6.31}$$

This system presents a generalization of anomalously diffusing systems in thermal baths with fat-tail memory [Morgado *et al.*(2002),Toussaint *et al.*(2006)]. It is interesting to see that an annealed-like noise arises from propagating the front through the quenched noise at a certain speed. Similarly to such anomalously diffusing systems, one can evaluate the amplitude of the Fourier mode after some time. From the auto-correlation function of a Fourier mode, averaging over starting time t_2, for a fixed time lag $t_1 - t_2$, one gets

$$\begin{aligned}\langle G_{kk'}(\Delta t)\rangle &= \langle\tilde{a}_k^*(t_2)\tilde{a}_{k'}(t_1)\rangle_{t_1,t_1-t_2=\Delta t} \qquad (6.32)\\ &= \lim_{T_2\to\infty}(T_2)^{-1}\int_0^{T_2} dt_2\int_{-\infty}^{t_1} dt'\int_{-\infty}^{t_2} dt''\\ &\quad \lambda^2\bar{v}^2\langle\delta\tilde{G}^*_{ck'}(t'')\delta\tilde{G}_{ck}(t')\rangle e^{\lambda\bar{v}\bar{G}|k|(t'+t''-t_1-t_2)}\end{aligned}$$

where the star denotes the complex conjugate. We will use the fact that the quenched disorder is uncorrelated above a size l_c, to approximate its Fourier transform along the front as the one obtained for a straight line traveling at speed $\bar{v}$ in this landscape:

Along such straight fronts at positions $(x', a_0 + \bar{v}t')$ and $(x'', a_0 + \bar{v}t'')$, the values of $G_c(x', t') = G_c(x', a_0 + \bar{v}t')$ and $G_c(x'', t'') = G_c(x'', a_0 + \bar{v}t'')$ correspond to a white noise of square amplitude σ^2_{Gc} that are correlated for spatial distances $|x' - x''| < l_c$, and time lags such that $\bar{(v)}|t' - t''| < l_c$ (l_c is defined as the correlation range of the quenched disorder). Hence, expressing this condition with a Heaviside function Θ as $\Theta(l_c - \bar{v}|t' - t''|)$, the resulting time integration Kernel in the equation above can be expressed as

$$\begin{aligned}&\langle G_c(x'', t'')G_c(x', t')\rangle \qquad (6.33)\\ &= \sigma^2_{Gc}\Theta(l_c - |x' - x''|)\Theta(l_c - \bar{(v)}|t' - t''|) \qquad (6.34)\\ &\simeq \sigma^2_{Gc}\Theta(l_c - |x' - x''|)l_c/\bar{v}\delta(t' - t''), \qquad (6.35)\end{aligned}$$

with $\delta(t' - t'')$ the Dirac function. In Fourier space, with discrete Fourier transform of steps l_c, this corresponds to

$$\langle\delta\tilde{G}^*_{ck'}(t'')\delta\tilde{G}_{ck}(t')\rangle = \sigma^2_{Gc}\delta_{kk'}l_c/\bar{v}\delta(t' - t''),$$

with $\delta_{kk'}$ the Kronecker symbol. We checked in the numerical model the validity of this approximation.

This can be used in Eq.6.32 to obtain the time correlation of the Fourier modes of the front shape:

$$\begin{aligned}\langle G_{kk'}(\Delta t)\rangle &= \langle\tilde{a}_k^*(t_2)\tilde{a}_{k'}(t_1)\rangle_{t_1,t_1-t_2=\Delta t} \qquad (6.36)\\ &= \lim_{T_2\to\infty}(T_2)^{-1}\int_0^{T_2} dt_2\int_{-\infty}^{t_1} dt'\int_{-\infty}^{t_2} dt''\\ &\quad \lambda^2\bar{v}^2\sigma^2_{Gc}\delta_{kk'}l_c/\bar{v}\delta(t' - t'')e^{\lambda\bar{v}\bar{G}|k|(t'+t''-t_1-t_2)}\\ &= \lim_{T_2\to\infty}(T_2)^{-1}\int_0^{T_2} dt_2\lambda^2\bar{v}\sigma^2_{Gc}\delta_{kk'}l_c\int_{-\infty}^{t_2} dt''\\ &\quad e^{\lambda\bar{v}\bar{G}|k|(-2t_2+2t''-\Delta t)}\\ &= \lim_{T_2\to\infty}(T_2)^{-1}\int_0^{T_2} dt_2\lambda^2\bar{v}\sigma^2_{Gc}\delta_{kk'}l_c\int_{-\infty}^{0} dt'''e^{\lambda\bar{v}\bar{G}|k|(2t'''-\Delta t)}\end{aligned}$$

This leads to the auto-correlation function of the front shape after time has led it to saturation:

$$\langle G_{kk'}(\Delta t)\rangle = \lambda\sigma_{Gc}^2\delta_{kk'}l_c/(2\bar{G}|k|)e^{-\lambda\bar{v}\bar{G}|k|\Delta t}. \tag{6.37}$$

The decorrelation time of these Fourier modes is thus scale dependent, with $T_d(k) = 1/\lambda\bar{v}\bar{G}|k|$. The amplitude of the k wave-mode of the front shape is given as

$$\langle ||\tilde{a}_k(t)||^2\rangle = G_{kk}(0) = \lambda\sigma_{Gc}^2 l_c/(2\bar{G}|k|). \tag{6.38}$$

This corresponds to a self affine behavior with a Hurst exponent 0, as predicted for elastic lines in annealed noise, as e.g. analyzed by [Perrin & Rice(1994),Favier *et al.*(2006)], i.e. a total amplitude for points at separation ΔL along the front scaling logarithmically as $W(\Delta L) \sim \log(\Delta L)$. For the elastic interactions for these large scale modes, from Eq. (6.2), this leads to

$$\begin{aligned} P_G(k) &= \bar{G}^2||\tilde{\gamma}_k||^2 \\ &= \bar{G}^2|k|^2||\tilde{a}_k||^2 \\ &= \lambda\sigma_{Gc}^2 l_c\bar{G}|k|/2. \end{aligned} \tag{6.39}$$

Assuming that the effective average value of G during propagation scales as the average value μ_{G_c} of the quenched disorder G_c, one gets

$$P_G(k) = \lambda l_c\sigma_{Gc}^2\mu_{G_c}|k|/2. \tag{6.40}$$

This is indeed the scaling found for small k: the amplitude of the Fourier transform of the energy release rate is proportional to k for large wavelengths, and this theory explains the numerical findings for the prefactor, i.e. that $P_G(k) = C\lambda\sigma_{Gc}^2\mu_{G_c}|k|$.

According to these analytical considerations, for small k, we have $||\tilde{\gamma}_k|| \ll ||\delta\tilde{G}_{ck}||/\bar{G}$, and the front propagates similarly to an elastic line in an annealed noise of average μ_{G_c}, fluctuations of standard deviation σ_{Gc}, and time correlation $l_c/\bar{v}$ (Figure 8). For larger k, the argument of the exponential in the Arrhenius law saturates, so that $||\tilde{\gamma}_k|| \sim ||\delta\tilde{G}_{ck}||/\bar{G}$: the small scale (large k) wave-modes are pinned on the quenched disorder, and the front propagation is similar to that of a quasistatic elastic line model: this corresponds to a flat spectrum of the energy release rate at a characteristic level $P_G(k) \sim \sigma_{G_c}^2$; and the front presents a Hurst exponent of $1/2$ (Figure 8).

The system toggles between annealed and quenched behavior at the scale where the energy spectrum becomes comparable to the large k saturation value, i.e. at a characteristic scale $2\pi/k_c$, so that

$$P_G(k_c) = \lambda l_c\sigma_{Gc}^2\mu_{G_c}|k_c|/2 = \sigma_{G_c}^2, \tag{6.41}$$

i.e.

$$k_c = 2/(l_c\lambda\mu_{G_c}). \tag{6.42}$$

These scalings for the power spectrum of G allow to predict a collapse for the power spectra of the energy release rate, as $P_G(k)/\sigma_{G_c}^2$ as function of k/k_c:

$$\begin{aligned} P_G(k)/\sigma_{G_c}^2 &= |k|/k_c \quad \text{for} \quad k/k_c \ll 1 \\ P_G(k)/\sigma_{G_c}^2 &= 1 \quad \text{for} \quad k/k_c \gg 1 \end{aligned} \tag{6.43}$$

Indeed, all simulations collapse on the predicted scaling function, as seen on Fig. 9. For the shape of the front, this scaling predicts the following collapse of the Fourier power spectra of the front shape $a(x)$:

$$\begin{aligned} k_c^2\langle G\rangle^2 P_a(k)/\sigma_{G_c}^2 &= k_c/|k| \quad \text{for} \quad k/k_c \ll 1 \\ k_c^2\langle G\rangle^2 P_a(k)/\sigma_{G_c}^2 &= (k_c/|k|)^2 \quad \text{for} \quad k/k_c \gg 1 \end{aligned} \tag{6.44}$$

Indeed, all simulations collapse in this representation, on scaling functions corresponding to these predicted prefactors, as seen on Fig. 7.

Recalling that $\lambda = \alpha^2/k_BT$ with α a characteristic size between breaking elements projected over the average plane, k_B the Boltzmann constant and T the absolute temperature (in kelvins),

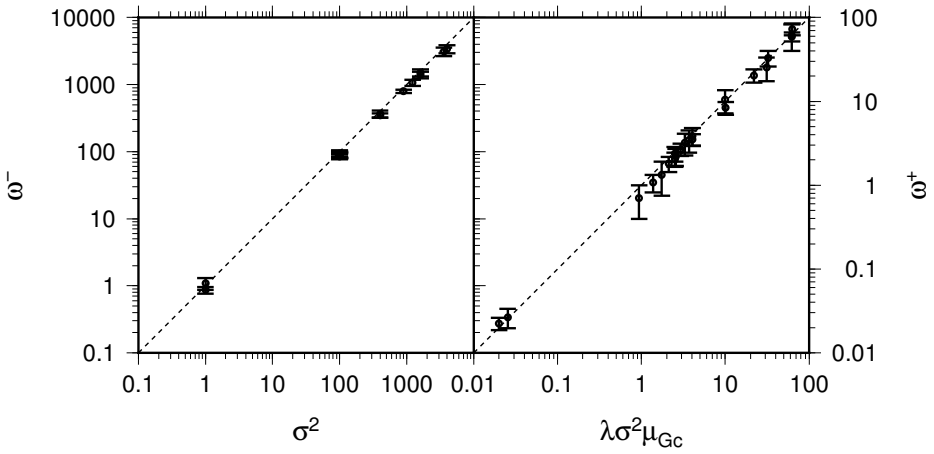

Figure 8. Comparisons between the predicted values of the energy release rate power spectrum $P_G(k)$ and the observed values in the simulations. Predictions of the values of $P_G(k)$ are given at large scale by Eq. (6.40) and are compared to values extracted from simulations results ω^+. At small scale analytical results predicted by Eq. (6.20) are compared to the values ω^- corresponding to the plateau $P_G(k)$ in simulations.

and that l_c is the correlation length of the quenched disorder and μ_{G_c} its average value, the critical length in the system is

$$R_c = 2\pi/k_c = \pi l_c \alpha^2 \mu_{G_c}/(k_B T). \tag{6.45}$$

Above this size, the system is dominated by thermal fluctuations (i.e. it behaves as if the noise was annealed), and below it is essentially pinned by the quenched noise: indeed, we have established above that for scales below R_c, (k larger than k_c), the self affine character of the morphology comes from an equilibrium between the elastic interactions and the quenched disorder ($||\tilde{\gamma}_k|| \sim ||\delta\tilde{G}_{ck}||/\bar{G}$), as in a quasistatic model. Conversely, for the scales above R_c, (k smaller than k_c), the elastic interaction term is small ($||\tilde{\gamma}_k|| \ll ||\delta\tilde{G}_{ck}||/\bar{G}$), the dynamic equation for the Fourier mode of the front $a_k(t)$ can be linearized, and the dynamics corresponds to the linear response of an elastic line in an annealed noise - where this pseudo thermal noise arises from sampling the quenched noise with a homogeneously advancing front.

Around this scale R_c, the front shape deviates from the small scale self affine scaling with a Hurst exponent of 0.5, with a progressive flattening of the slope in Fourier mode. This could be the origin of the smoothening observed at large scales, as reported in [Santucci *et al.*(2010)]. For the experimentally determined values $\lambda = \alpha^2/k_B T \sim 0.13\,\mathrm{m}^2/\mathrm{J}$, $\mu_{G_c} = 200\,\mathrm{J/m}^2$, and a correlation size of the quenched disorder $l_c = 2.8\,10^{-2}/2048\mathrm{m} \simeq 13.7\,\mu\mathrm{m}$, this corresponds to a critical value R_c around 1 mm. This corresponds indeed to the cross over values seen in Figs. 6 and 7. This also corresponds, in order of magnitude, to the experimental range, where a softening of the front scaling is found [Santucci *et al.*(2010)].

7. Discussion

The results of our numerical simulations show a good agreement with various experimental observations. We first documented at the macroscopic scale the propagation of the crack that well renders an Arrhenius law behavior defined by Eq. (6.1) and observed experimentally. It is noteworthy that even when the elastic energy at the crack tip is lower than a critical threshold (similar to a Griffith energy criterion) we reproduce the propagation of the crack. This creeping behavior results from the introduction of a finite temperature in the model compared to quasi-static simulation defined at $T = 0$. Our results show that the global response of the system is

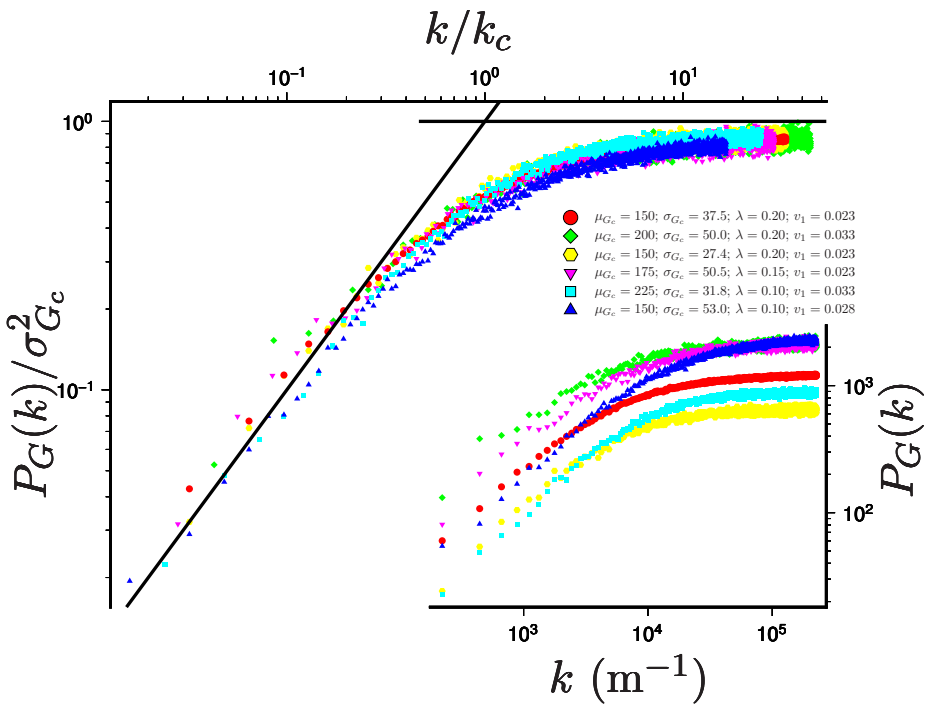

Figure 9. Power spectra of the energy release rate, $P_G(k)$, computed for different simulations (insert). Units of the parameters in the legend are for G_c, Jm^{-2}, for λ, m^2/J and for v_1, m/s. (Main:) When the spectrum is rescaled by $\sigma^2_{G_c}$, and the wavenumbers as k/k_c with $k_c = 2/(l_c \lambda \mu_{G_c})$, the power spectra collapse, according to the theory. The two continuous lines correspond to $P_G(k)/\sigma^2_{G_c} = 1$ and $P_G(k)/\sigma^2_{G_c} = k/k_c$.

similar to the local response imposed at the mesoscale, providing that the fluctuations of the interface disorder are not too high.

As a second step we turned to comparisons between simulations and experiments at the local scale. We showed that the shape of the local front velocities distribution is governed by a parameter $\rho = \mu^2_{G_c}/(\sigma^2_{G_c}\lambda)$, with $\lambda = \alpha^2/k_B T$. The higher the relative disorder fluctuation term (σ_{G_c}/μ_{G_c}) or the lower the temperature, T, the broader the distribution of local speed. Extrapolating ρ to a very low value will then produce a very intermittent activity with very fast movements and long repose periods of local velocity. This is expected when the thermal rounding is very sharp and is similar to a pinning regime. On the other side, for high values of ρ, i.e. for high temperature or low disorder fluctuations, the velocity becomes more homogeneous and local sites along the front are all propagating around the mean crack velocity. For a set of parameters corresponding to the one encountered experimentally we have shown that we are able to reproduce the correct shape of the velocity distribution, notably we reproduce the correct power law decay of the pdf tail with exponent $\eta = -2.55$. It is remarkable to note that that such power-law decay is a very robust experimental observation. Indeed, if one interprets this result in light of our simulations, changing significantly the shape of the velocity distribution requires an important change of the experimental condition (for example a fourfold decrease of the absolute temperature for the case reported in Figure 6).

We made a final comparison between our simulations and experimental data concerning the morphology of the crack front line. We showed that our simulations display a crack front morphology with a cross-over length separating two regimes : a regime with a Hurst exponent $\zeta^+ = 0.0$ at large scale and a regime with a higher Hurst exponent $\zeta^- = 0.5$ at a smaller scale. This cross over between two regimes has also been reported experimentally, with the transition

to a higher Hurst exponent at small scale [Santucci *et al.*(2010)]. We notice that there still exists a difference between exponents obtained in our simulations and those observed in experiments. Distinguishing if this discrepancy arises from a limited resolution on the experimental data or if other phenomena may have been neglected in our model is difficult to assess. We nevertheless obtained estimates of the roughness exponents quite close to the experimentally observed ones. Furthermore the cross-over length scale reported in our simulations is in the correct order of magnitude compared to the one described in experiments. Results of our simulations concerning roughness exponents of the crack front are also validated by theoretical derivations from the Arrhenius model. This theoretical analysis also leads us to determine the physical mechanism operating above or below the cross-over length R_c. In a first regime, at large scale, elastic interactions are well below the quenched noise amplitude and the front propagates similarly to an elastic line in an annealed noise. At smaller scale, below R_c, elastic interactions are balancing quenched noise amplitude and the front propagation is similar to that of a quasistatic elastic line model. We note that the quasistatic elastic line model gives a Hurst exponent $H = 0.35 - 0.39$, somewhat lower than the value obtained here at small scale (e.g. [Schmittbuhl *et al.*(1995)]). However in this model and in the regime of small fluctuations of the crack front line, the Hurst exponent gets a higher value $H = 0.5$, similar to the one found here [Schmittbuhl & Vilotte(1999)]. It suggests that in the small scale regime, our model is similar to the elastic line model in the presence of small fluctuations. A speculative explanation for this observation is related to the different dynamics between our model and the quasistatic elastic line model. In our model, all points along the crack front line are moving at each time step maintaining the crack front line in an equilibrium position at each time step. In the quasistatic elastic line model, only one point is advanced at a time and reaches its new equilibrium position. The dynamics of the crack front line introduced in our model could thus be an explanation for the $H = 0.5$ exponent rather than the value $H = 0.35 - 0.39$.

Recent studies have suggested that the use of the elastic kernel as proposed in [Gao & Rice(1989)] should be taken cautiously as it is limited to the approximation of an infinite medium [Legrand *et al.*(2011)]. Finiteness of the medium is suspected to have an influence on the reported scaling. However the shape of the elastic kernel computed in [Legrand *et al.*(2011)] is the same as in the infinite case for range of interactions smaller than the plate thickness. Since the experimental data available and compared to the current model are essentially in a scale range equal or smaller than the thickness, this justifies that the modifications of the kernel due to finite thickness can be neglected. Preliminary simulations incorporating the elastic kernel computed in [Legrand *et al.*(2011)] that accounts for the finiteness of the elastic medium, i.e. for the limited thickness of the PMMA plate, confirm the validity of this approximation (but analyzing what happens at large scales, above the thickness, is beyond the scope of the current paper).

A limitation of our study is that it is restricted to cracks propagating at low velocities. This choice of restricting our simulation to slow speeds is motivated by the main purpose of this article which aims at comparing the results of the model with experimental crack propagating in the same velocity range. Although no influence of the velocity was observed on the reported scaling during our simulations, it is possible that such effects might appear at higher speeds. It is also readily possible that other effects may manifest at higher speeds when approaching the rupture velocity of the material. In particular, at the local scale, dynamic rupture might take place, as observed experimentally by the recording of acoustic emissions [Lengliné *et al.*(2012)], and might influence the crack propagation by redistributing elastic stress [Ramanathan & Fisher(1998)]. In our simulations we did not consider any dynamic effect and implicitly hypothesized that these dynamics effects have a limited influence on the tested crack front features. Limiting the complexity of our model also allows us to track more easily any individual effect induced by each of its parameters. We also show that, despite its simplicity, our model is able to reproduce all reported robust experimental features.

A second approximation made in our model is the hypothesis of a homogeneous and constant temperature field. It is indeed quite likely that the fracturation process in experiments

release some heat at the crack tip as observed in PMMA [Fuller *et al.*(1975)]. Local increases of temperature have the ability to change the local crack propagation speed in our model as defined by Eq. 2.8. However we hypothesized that at the scale of investigation this effect can be ignored in our model. Temperature increase of a few degrees around crack tips was observed or modeled in the case of fatigue in steel ([Ranc *et al.*(2014)]), or locally tenth of degrees or more in the case of fracture in paper ([Toussaint *et al.*(2016)]). This choice of negligible temperature increase at the crack tip in the current model was done for simplicity as a first approximation, and is shown to produce some agreement with the experimental observations. Incorporating the impacts of crack tip temperature elevation is the subject of ongoing further research.

It is also likely that other processes, not taken into account in our model, play some role on the propagation of cracks in heterogeneous media and may also offer alternative explanations for some of the observed features. For example, it is noteworthy that [Bonamy *et al.*(2008),Santucci *et al.*(2018)] were able to capture some of the experimental features exposed here, as the velocity distribution, while not considering the effect of temperature in the crack propagation. The model of ([Laurson *et al.*(2010)]) coud also capture two scaling laws in the front morphology. The cross-over length found there, proportional to the Larkin length, differed from the one identified in the model presented here. Interestingly, a recent model of interfacial crack propagation was also able to capture much of the experimental data tested here (velocity distribution and roughness exponent) [Gjerden *et al.*(2013)]. In this model, the cross over of the roughness exponent is related to the transition from a percolation regime at small scale (giving $H = 2/3$) to an elastic line model at larger scale ($H = 0.39$). It thus remains to distinguish at which scale each of this mechanism is governing the scaling of the front morphology. This investigation is left for further study.

The results of this model can also be analyzed in the light of the classification between strong pinning regime and weak pinning regime, reported for elastic lines propagating with a Paris law creep rheology [Lazarus(2011)]. For these models, smooth values of quenched disorder map lead to a dynamics where $G = G_c$ (or equivalently, $K = K_c$, with K the stress intensity factor) all along the front: this is termed the weak pinning regime. On contrary, for quasi-static models (as e.g. in [Schmittbuhl *et al.*(1995)]), a behavior where $G \leq G_c$ (or $K \leq K_c$) is observed, which is termed the strong pinning regime, and attributed to sharp transitions in quenched disorder [Lazarus(2011)]. With respect to this classification, the model presented in the current manuscript is neither in the weak nor in the strong pinning regime, but rather in one or the other depending on the scales considered: as shown above, the front at small scales follows a weak pinning regime behavior, with a scaling dictated by $\tilde{G}_k \simeq \tilde{G}_{ck}$ for $k > k_c$. On contrary, at large scales, for $k < k_c$, the scaling is dictated by the thermal noise rather than the quenched disorder, and one has $||\tilde{G}_k|| \ll ||\tilde{G}_{ck}||$, which in the terminology of [Lazarus(2011)], corresponds to a strong pinning behavior. The exact scaling at these large scales, as shown in the previous sections, can be computed from the diffusion of an elastic line in a thermal noise.

Our model have been intentionally limited to a 1D line model in order to test the results of our simulations with experimental observations of *in-situ* crack propagation. It is appealing to generalize the results of our model to higher dimension systems and in particular to fault systems. Discussing our results in terms of fault mechanics provide an insight into the notion of seismic coupling. The seismic coupling coefficient is defined as the ratio of seismic to aseismic deformation on a fault plane in a bounded geographical area. In our configuration, if one accepts to extrapolate the computed velocity distribution to dynamic rupture speed, then the ratio of seismic to aseismic deformation would be given by the level of the distribution tail in the range of dynamic speed. As we have shown, this level is governed by the parameter ρ. Linking our geometrical configuration to a simple 1D fault model as proposed in [Perfettini *et al.*(2003),Schmittbuhl *et al.*(2003)] we can thus interpret our results in terms of slip on faults. In particular our results give a possible interpretation for this notion of seismic coupling with the introduction of the coefficient ρ. This coefficient is shown to vary with temperature which exhibits large scale variations within the Earth. It is also proposed to vary with the amplitude of the toughness heterogeneities on the fault plane, due for example to the presence of asperities on

the interface. Such conclusions are in agreement with the conceptual model proposed in [Bourouis & Bernard(2007)].

8. Conclusion

In conclusion we presented a model of crack propagation in heterogeneous media governed by an Arrhenius law. Despite its simple expression, we showed that our model is in full agreement with all reported features of interfacial crack front propagation in the presence of disorder (morphology, speed distribution and macroscopic dynamics): the speed distribution is found to present a non Gaussian power law tail $p(v) \sim v^{-2.6}$. The front morphology is found to obey a self affine scaling with a Hurst exponent around $H \sim 0.5$ at small scales, and a cross over to $H \sim 0$ at large scales. These features are different from purely quasi-static models, where only quenched noise is included, without the thermal part: indeed, in such models, the power law distribution of the local speeds has not been obtained, no large scale flattening is observed. In contrast with quasi-statis models, our model also predicts the creep behavior, i.e. the correct non zero large-scale velocity at fixed loading.

The parameters inferred in our model which best reproduce the experimental observations correspond to realistic values encountered during experiments. Our numerical results are supported by an analytical analysis explaining why thermal noise plays a role at large scales and why quenched disorder plays a role at small scales. This theoretical development also predicts both scaling regimes of the crack shape, and how the cross-over scale depends on the characteristics of the disorder, on the size of the breaking elements, and on temperature. We also showed that the existence of a parameter, $\rho = \mu_{G_c}^2 k_B T/(\sigma_{G_c}^2 \alpha^2)$, governs the shape of the local speed distribution. This parameter is defined from the temperature of the system T, a size connected to the individual breaking molecular bonds α, and the relative fluctuations of the quenched disorder σ_{G_c} with respect to the characteristic energy release rate μ_{G_c}. We finally emphasize that our results explain why even in the presence of disorder, macroscopic observations of slow crack growth are well modeled by an Arrhenius relation, and highlight the importance of thermal fluctuations in governing the propagation of crack which yields characteristic properties not only at a global scale but also at a small scale. It also opens some possibility of inverting physical parameters related to the crack environment from the observation of its dynamical and morphological features.

Ethics. No crack front nor computer was harmed during this study.

Data Accessibility. The numerical code is accessible upon request to the authors.

Authors' Contributions. RT, AC, OL and KJM stated the basis of the model. AC wrote the numerical model. AC and OL ran the model and generated the figures. RT performed the analytical developments together with KJM. RT, OL, AC and KJMwrote the text. All authors read and approved the manuscript'.

Competing Interests. The author(s) declare that they have no competing interests.

Funding. The authors acknowledge the support of the LIA France-Norway D-FFRACT, the Universities of Strasbourg and Oslo, the CNRS-INSU, the ITN FLOWTRANS and the ANR LANDQUAKE. This work was partly supported by the Research Council of Norway through its Centres of Excellence funding scheme, project number 262644.

Acknowledgements. The authors thank S. Santucci, T. Vincent-Dospital, E.G. Flekkøy, K.T. Tallakstad, A. Hansen and L. Ponson for insightful discussions.

References

Anderson(1995) Anderson, T. L. 1995 *Fracture mechanics - Fundamentals and applications*, 2nd edn. Boca Raton, FL: CRC press.

Atkinson(1987) Atkinson, K. 1987 *Fracture mechanics of rocks*. London, UK: Academic press limited.

Ben-Zion & Morrissey(1995) Ben-Zion, Y., & Morrissey, J. 1995. A simple re-derivation of logarithmic disordering of a dynamic planar crack due to small random heterogeneities.
Journal of the Mechanics and Physics of Solids, **43**(9), 1363 –1368.

Bonamy & Bouchaud(2011) Bonamy, D. & Bouchaud, E. 2011 Failure of heterogeneous materials: A dynamic phase transition?
Physics Reports, **498**(1), 1 – 44.
(doi:http://dx.doi.org/10.1016/j.physrep.2010.07.006)

Bonamy *et al.*(2008) Bonamy, D., Santucci, S. & Ponson, L. 2008 Crackling Dynamics in Material Failure as the Signature of a Self-Organized Dynamic Phase Transition.
Physical Review Letters, **101**(4), 045 501–+.
(doi:10.1103/PhysRevLett.101.045501)

Bouchaud(1997) Bouchaud, E. 1997 Scaling properties of cracks.
Journal of Physics Condensed Matter, **9**(21), 4319–4344.
(doi:10.1088/0953-8984/9/21/002)

Bourouis & Bernard(2007) Bourouis, S. & Bernard, P. 2007 Evidence for coupled seismic and aseismic fault slip during water injection in the geothermal site of soultz (france), and implications for seismogenic transients.
Geophysical Journal International, **169**(2), 723–732.

Bustingorry *et al.*(2008) Bustingorry, S., Kolton, A. & Giamarchi, T. 2008 Thermal rounding of the depinning transition.
Europhys. Lett., **812**(26005).

Chauve *et al.*(2000) Chauve, P., Giamarchi, T. & Le Doussal, P. 2000 Creep and depinning in disordered media.
Physical Review B - Condensed Matter and Materials Physics, **62**(10), 6241–6267.

Chen & Marchetti(1995) Chen, L.-W. & Marchetti, M. C. 1995 Interface motion in random media at finite temperature.
Physical Review B, **51**(10), 6296.

Cochard & Rice(1997) Cochard, A. & Rice, J. R. 1997 A spectral method for numerical elastodynamic fracture analysis without spatial replication of the rupture event.
Journal of the Mechanics and Physics of Solids, **45**(8), 1393–1418.

Delaplace *et al.*(1999) Delaplace, A., Schmittbuhl, J. & Måløy, K. J. 1999 High resolution description of a crack front in a heterogeneous plexiglas block.
Phys. Rev. E, **60**(2), 1337–1343.
(doi:10.1103/PhysRevE.60.1337)

Favier *et al.*(2006) Favier, E., Lazarus, V. & Leblond, J.-B. 2006 Statistics of the deformation of the front of a tunnel-crack propagating in some inhomogeneous medium.
Journal of the Mechanics and Physics of Solids, **54**(7), 1449–1478.

Frigo & Johnson(2005) Frigo, M. & Johnson, S. 2005 The design and implementation of fftw3.
Proceedings of the IEEE, **93**(2), 216–231.

Fuller *et al.*(1975) Fuller, K., Fox, P. & Field, J. E. 1975 The temperature rise at the tip of fast-moving cracks in glassy polymers.
Proc. R. Soc. Lond. A, **341**(1627), 537–557.

Gao & Rice(1989) Gao, H. & Rice, J. R. 1989 A first-order perturbation analysis of crack trapping by arrays of obstacles.
J. App. Mechanics, **56**, 828–836.

Gjerden *et al.*(2013) Gjerden, K., Stormo, A. & Hansen, A. 2013 Universality classes in constrained crack growth.
Physical Review Letters, **111**(13).

Hairer *et al.*(1993) Hairer, E., Nørsett, S. & Wanner, G. 1993 *Solving ordinary differential equations i. nonstiff problems*.
Springer-Verlag.

Kolton *et al.*(2009) Kolton, A. B., Rosso, A., Giamarchi, T. & Krauth, W. 2009 Creep dynamics of elastic manifolds via exact transition pathways.
Physical Review B, **79**(18), 184 207.

Lawn(1993) Lawn, B. 1993 *Fracture of brittle solids*.
Cambridge University Press, 2nd edn.

Laurson *et al.*(2010) Laurson, L., Santucci, S. & Zapperi, S. 2010 Avalanches and clusters in planar crack front propagation

Phys. Rev. E **81**, 046116.
(doi:DOI:10.1103/PhysRevE.81.046116)

Lazarus(2011) Lazarus, V. 2011 Perturbation approaches of a planar crack in linear elastic fracture mechanics: A review.
Journal of the Mechanics and Physics of Solids, **59**(1), 121–144.
(doi:DOI:10.1016/j.jmps.2010.12.006)

Legrand *et al.*(2011) Legrand, L., Patinet, S., Leblond, J.-B., Frelat, J., Lazarus, V. & Vandembroucq, D. 2011 Coplanar perturbation of a crack lying on the mid-plane of a plate.
International Journal of Fracture, **170**(1), 67–82.

Lengliné *et al.*(2012) Lengliné, O., Elkhoury, J., Daniel, G., Schmittbuhl, J., Toussaint, R., Ampuero, J.-P. & Bouchon, M. 2012 Interplay of seismic and aseismic deformations during earthquake swarms: An experimental approach.
Earth and Planetary Science Letters, **331-332**, 215–223.

Lengliné *et al.*(2011*a*) Lengliné, O., Schmittbuhl, J., Elkhoury, J., Ampuero, J.-P., Toussaint, R. & Måløy, K. 2011*a* Downscaling of fracture energy during brittle creep experiments.
Journal of Geophysical Research B: Solid Earth, **116**(8).

Lengliné *et al.*(2011*b*) Lengliné, O., Toussaint, R., Schmittbuhl, J., Elkhoury, J., Ampuero, J., Tallakstad, K., Santucci, S. & Måløy, K. 2011*b* Average crack-front velocity during subcritical fracture propagation in a heterogeneous medium.
Physical Review E - Statistical, Nonlinear, and Soft Matter Physics, **84**(3).

Måløy *et al.*(2006) Måløy, K. J., Santucci, S., Schmittbuhl, J. & Toussaint, R. 2006 Local waiting time fluctuations along a randomly pinned crack front.
Phys. Rev. Lett., **96**(4).

Morgado *et al.*(2002) Morgado, R., Oliveira, F., George Batrouni, G. & Hansen, A. 2002 Relation between anomalous and normal diffusion in systems with memory.
Physical Review Letters, **89**(10), 1006 011–1006 014.

Patinet *et al.*(2013) Patinet, S., Vandembroucq, D. & Roux, S. 2013 Quantitative prediction of effective toughness at random heterogeneous interfaces.
Physical Review Letters, **110**(16).
(doi:10.1103/PhysRevLett.110.165507)

Perfettini *et al.*(2003) Perfettini, H., Schmittbuhl, J. & Cochard, A. 2003 Shear and normal load perturbations on a two-dimensional continuous fault: 1. static triggering.
Journal of Geophysical Research B: Solid Earth, **108**(9), ESE 1–1 – 1–16.

Perrin & Rice(1994) Perrin, G. & Rice, J. 1994 Disordering of a dynamic planar crack front in a model elastic medium of randomly variable toughness.
Journal of the Mechanics and Physics of Solids, **42**(6), 1047–1064.

Perrin *et al.*(1995) Perrin, G., Rice, J. R. & Zheng, G. 1995 Self-healing slip pulse on a frictional surface.
Journal of the Mechanics and Physics of Solids, **43**(9), 1461–1495.

Pindra *et al.*(2009) Pindra, N., Lazarus, V., Leblond, J., Schmittbuhl, J. & Toussaint, R. 2009 Deformation of the crack front during propagation in some disordered medium: Theoretical and experimental studies.
vol. 8, pp. 6356–6364.

Ramanathan & Fisher(1998) Ramanathan, S. & Fisher, D. 1998 Onset of propagation of planar cracks in heterogeneous media.
Phys. Rev. B, **58**, 6026–6046.

Ranc *et al.*(2014) Ranc, N., Palin-Luc, T., Paris, P.C., Saintier, N. 2014 About the effect of plastic dissipation in heat at the crack tip on the stress intensity factor under cyclic loading,
International Journal of Fatigue, **58**, 56–65,
(doi:10.1016/j.ijfatigue.2013.04.012).

Pindra *et al.*(2009) Pindra, N., Lazarus, V., Leblond, J., Schmittbuhl, J. & Toussaint, R. 2009 Deformation of the crack front during propagation in some disordered medium: Theoretical and experimental studies.
12th International Conference on Fracture 2009, ICF-12, **8**, 6356–6364.

Rosso & Krauth(2002) Rosso, A. & Krauth, W. 2002 Roughness at the depinning threshold for a long-range elastic string.
Physical Review E - Statistical, Nonlinear, and Soft Matter Physics, **65**(2), 025 101/1–025 101/4.

Santucci *et al.*(2010) Santucci, S., Grob, M., Toussaint, R., Schmittbuhl, J., Hansen, A. & Maløy, K.J. 2010 Fracture roughness scaling: A case study on planar cracks.

EPL (Europhysics Letters), **92**(4), 44 001.

Santucci *et al.*(2018) Santucci, S., Tallakstad, K.T., Angheluta, L., Laurson, L.,Toussaint, R. & Måløy, K.J. 2018 Avalanches and extreme value statistics in interfacial crackling dynamics. *Phil. Trans. R. Soc. A*, 20170394. (doi:10.1098/rsta.2017.0394)

Schmittbuhl *et al.*(2003) Schmittbuhl, J., Delaplace, A., Måløy, K. J., Perfettini, H. & Vilotte, J. P. 2003 Slow Crack Propagation and Slip Correlations. *Pure and Applied Geophysics*, **160**, 961–976. (doi:10.1007/PL00012575)

Schmittbuhl & Måløy(1997) Schmittbuhl, J. & Måløy, K. J. 1997 Direct Observation of a Self-Affine Crack Propagation. *Physical Review Letters*, **78**, 3888–3891. (doi:10.1103/PhysRevLett.78.3888)

Schmittbuhl *et al.*(1995) Schmittbuhl, J., Roux, S., Vilotte, J.-P. & Måløy, K. J. 1995 Interfacial Crack Pinning: Effect of Nonlocal Interactions. *Physical Review Letters*, **74**, 1787–1790. (doi:10.1103/PhysRevLett.74.1787)

Schmittbuhl & Vilotte(1999) Schmittbuhl, J. & Vilotte, J.-P. 1999 Interfacial crack front wandering: influence of quenched noise correlations. *Physica A: Statistical Mechanics and its Applications*, **270**(1-2), 42–56.

Scholz(2002) Scholz, C. H. 2002 *The mechanics of earthquakes and faulting*. Cambridge University Press.

Tallakstad *et al.*(2011) Tallakstad, K. T., Toussaint, R., Santucci, S., Schmittbuhl, J. & Måløy, K. J. 2011 Local dynamics of a randomly pinned crack front during creep and forced propagation: An experimental study. *Phys. Rev. E*, **83**(4), 046 108.

Tallakstad *et al.*(2013)Tallakstad, Toussaint, Santucci & Måløy Tallakstad, K., Toussaint, R., Santucci, S. & Måløy, K.J. 2013 Non-gaussian nature of fracture and the survival of fat-tail exponents. *Physical Review Letters*, **110**(14), 145501.

Toussaint *et al.*(2004) Toussaint, R., Helgesen, G. & Flekkøy, E. 2004 Dynamic roughening and fluctuations of dipolar chains. *Physical Review Letters*, **93**(10), 108 304–1–108 304–4.

Toussaint *et al.*(2006) Toussaint, R., Flekkøy, E. & Helgesen, G. 2006 Memory of fluctuating brownian dipolar chains. *Physical Review E - Statistical, Nonlinear, and Soft Matter Physics*, **74**(5).

Toussaint *et al.*(2016) Toussaint, R., Lengliné, O., Santucci, S., Vincent-Dospital, T., Naert-Guillot, M. & Måløy, K.J. 2016 How cracks are hot and cool: A burning issue for paper. *Soft Matter*, **12**(25), 5563-5571. (doi:DOI:10.1039/c6sm00615a)

Vandembroucq *et al.*(2004) Vandembroucq, D., Skoe, R. & Roux, S. 2004 Universal depinning force fluctuations of an elastic line: Application to finite temperature behavior. *Physical Review E*, **70**(5), 051 101.